TRANSIENT AND PSEUDOSTEADY-STATE PRODUCTIVITY OF HYDRAULICALLY FRACTURED WELL

A Thesis

by

ARDHI HAKIM LUMBAN GAOL

Submitted to the Office of Graduate Studies of
Texas A&M University
in partial fulfillment of the requirements for the degree of

MASTER OF SCIENCE

August 2012

Major Subject: Petroleum Engineering

Transient and Pseudosteady-State Productivity of Hydraulically Fractured Well

TRANSIENT AND PSEUDOSTADY-STATE PRODUCTIVITY OF HYDRAULICALLY FRACTURED WELL

A Thesis

by

ARDHI HAKIM LUMBAN GAOL

Submitted to the Office of Graduate Studies of
Texas A&M University
in partial fulfillment of the requirements for the degree of

MASTER OF SCIENCE

Approved by:

Chair of Committee,	Peter P. Valkó
Committee Members,	Christine E. Economides
	Yuefeng Sun
Head of Department,	A. Daniel Hill

August 2012

Major Subject: Petroleum Engineering

ABSTRACT

Transient and Pseudosteady-state Productivity of Hydraulically Fractured Well.

(August 2012)

Ardhi Hakim Lumban Gaol, B. Tech, Bandung Institute of Technology, Indonesia

Chair of Advisory Committee: Dr. Peter P. Valkó

Numerical simulation method is used in this work to solve the problem of transient and pseudosteady-state flow of fluid in a rectangular reservoir with impermeable boundaries. Development and validation of the numerical solution for various well-fracture configurations are the main objectives of this research. The specific case of horizontal well intersected by multiple transverse fractures is the focus of the investigation.

The solutions for different operating conditions, constant rate and constant pressure, are represented in the form of transient – peudosteady-state productivity indices. The numerical simulator is validated by comparing results to known analytical solution for radial flow, existing models of productivity for vertical well intersected by vertical fracture, and also with published tables of shape factors.

Numerical simulation is a powerful tool to predict well performance. The complexities of well-fracture configurations can be modeled in a truly 3-dimensional system and the pressure and productivity responses for all of the flow regimes can be computed efficiently, enabling optimization of the well-fracture system.

DEDICATION

This thesis is dedicated to:

My mother, Sri Roediharti

My father, Anipar Lumban Gaol

ACKNOWLEDGEMENTS

I would never have been able to finish my thesis without the guidance of my committee members, great help from my colleagues and support from my family and friends. I am heartily thankful to my supervisor, Dr. Valkó, whose encouragement, guidance and support enabled me to develop an understanding of the subject. My greatest appreciation also goes to Dr. Economides and Dr. Sun for the help and support as my committee members.

I would like to thank to the Chevron Indonesia Co. and Bandung Institute of Technology (Indonesia) that has provided a financial support for my Master study in Texas A&M University.

NOMENCLATURE

C_{fD} = dimensionless fracture conductivity

c_o = oil compressibility, Lt^2/m, 1/psi

c_{te} = total effective compressibility, Lt^2/m, 1/psi

I_x = lateral fracture penetration ratio

J_D = dimensionless productivity index

k = permeability, L^2, md

k_f = fracture permeability, L^2, md

n_f = number of fractures

p = pressure, m/Lt^2, psi

p_{ave} = average reservoir pressure, m/Lt^2, psi

p_D = dimensionless pressure

p_i = initial reservoir pressure, m/Lt^2, psi

p_{ref} = reference pressure, m/Lt^2, psi

p_{wf} = wellbore flowing pressure, m/Lt^2, psi

PI = Productivity Index, L^4/tm, bbl/d/psi

q = production rate, L^3/t, bbl/d

q_o = oil production rate, L^3/t, bbl/d

q_w = water production rate, L^3/t, bbl/d

Q = qumulative production, L^3, bbl

r_D = dimensionless radius

r_w = wellbore radius, L, ft

s = skin

t = time, t, day

T = temperature, T, F

t_D = dimensionless time

t_{DA} = dimensionless time with regard to reference drainage area

u = Laplace parameter

w = fracture width, L, ft

x_D = dimensionless point in x-direction

xe = reservoir length, L, ft

x_f = fracture half length, L, ft

x_0 = gridblock size of the well location, L, ft

V_f = fracture volume, L^3, ft^3

V_{res} = reservoir volume, L^3, ft^3

y_e = reservoir width, L, ft

z_e = reservoir height, L, ft

α = conversion factor

μ = fluid viscosity, m/Lt, cp

ρ = fluid density, m/ L^3, lbm/ft^3

ρ_o = oil density, m/ L^3, lbm/ft^3

ρ_{ref} = reference density, m/ L^3, lbm/ft^3

ϕ = porosity, fraction

TABLE OF CONTENTS

CHAPTER Page

LIST OF FIGURES

FIGURE Page

FIGURE Page

LIST OF TABLES

CHAPTER I

INTRODUCTION

1.1 Statement of The Problem

Completing the horizontal well by creating multiple transverse fractures is a common practice in tight formations. This type of completion is is being applied in the field in order to produce oil or gas at economical rates. Hydraulic fracturing of horizontal well is also recommended if the formation has restricted vertical flow, because of low vertical permeability or the presence of shale or clay streaks in the formation.

The overall objective of this study is to quantify the transient and pseudosteady-state productivity of the well-fracture system in a rectangular reservoir with closed boundaries. The approach is based on 3-dimensional reservoir simulator, developed for this purpose. This obtained solution should be directly applicable to fracture design and analysis, especially for complex well-fracture systems, such as horizontal well intersected with transverse fractures. Special emphasis is placed on additional pressure drop due to limited contact area between the well and the fractures. The results are represented in the form of transient and pseudosteady-state productivity index, providing a tool for completion design and optimization.

This thesis follows the style of *SPE Journal*.

Reservoir simulation studies are carried out to calculate the productivity and long time performance of this system. The performance of horizontal well with transverse fractures is compared to a fractured vertical well. The factors involved in determining the optimum number of transverse fractures is also discussed.

The results of this study should be suitable for various tasks, including the prediction and analysis of early-time and long-time performance of horizontal well with multiple fractures and the optimum design of such a system under various economic and technical constraints.

1.2 Literature Review

In this section, the basic idea of hydraulic fracturing technology will be reviewed. Many conference and journal papers are available reporting methods to predict the performance of hydraulically fractured well, both vertical and horizontal. Various mathematical models have been suggested to predict the performance of such well-fracture configurations.

Gringarten *et al.* (1974) investigated the pressure distribution created by the vertical well intersected by an infinite-conductivity fracture. They subdivided the fracture into multiple segments and assumed that each segment acts as a uniform-flux source. The "analytical" solution was derived for constant rate operating condition to calculate the pressure distribution within the reservoir and the contribution from each fracture segment to the total production rate.

Cinco Ley *et al*. (1977) developed a mathematical model to solve the transient pressure behavior for a well with a finite-conductivity vertical fracture in an infinite slab

reservoir. It was assumed that fracture flux has a stepwise distribution in time and space, thus the finite-conductivity fracture was discretized into multiple segments and time was divided into different intervals. Flow distribution along the fracture was also investigated and compared with the infinite-conductivity solution of Gringarten *et al*.

The success of technology has increasing the productivity by inducing a single transverse fracture. Mukherjee and Economides (1991) pointed out that the fractured horizontal well can be treated as a "choked" vertical fracture due to limited contact between the well and fracture. This quantified this choking effect as an additional pressure loss around the wellbore.

Chen and Raghavan (1997) developed algorithms to compute the productivity of horizontal well with multiple transverse fractures in rectangular drainage area by using the reformulation of the Ozkan and Raghavan (1991) point-source solution. That solution was used later by Raghavan *et al*. (1997) to predict long time performance of the system with transverse and longitudinal fractures.

Economides *et al*. (2002) in their book introduced an optimization technique to obtain the optimum fracture dimensions providing maximum productivity. They consolidated two parameters: the fracture penetration ratio and the dimensionless fracture conductivity into one parameter which was termed proppant number. The proppant number represents the ratio between propped fracture and reservoir volumes. There is a unique maximum productivity index for each proppant number, and that can be realized by a unique optimum fracture width and length. Later, Romero and Valko (2003) developed a solution technique to calculate productivity in vertically fractured well by using direct boundary element method under pseudosteady-state condition. The

fracture was discretized into multiple line sources, the pressure drawdown between observation points was computed and flux distribution along the fracture could be determined. This method will be used later in this study as a basis of comparison to validate the new numerical simulator.

Al-Kobaisi *et al*. (2006) presented a hybrid numerical/analytical model for the pressure transient response of horizontal well with finite-conductivity transverse fracture. They coupled the analytical solutions for reservoir and fracture flows and used a numerical approach to obtain the pressure and flux distributions along the fracture.

The reservoirs is usually assumed to have a rectangular geometry instead of cylindrical.. Valko and Amini (2007) introduced the method of distributed volumetric sources (DVS) to solve transient and pseudosteady-state flow in a closed rectangular reservoir. This method assumes that the sources are 3-dimensional in the form of rectilinear volumes. Daal and Economides (2006) also investigated the performance of fractured well in rectangular drainage area. They presented the effect of the drainage shape on the productivity and formalized the optimization technique based on the concept of proppant number for various reservoir geometry and number of fractures.

1.3 Research Objective and Approach

The overall objectives of this study are:

- To develop and validate a numerical simulation tool to determine the solution for pressure and production behavior of hydraulically fracture fractured well in a rectangular drainage volume bounded by closed boundaries.

- To use the methodology for predicting the transient and pseudosteady-state productivity index behavior.
- To apply the method of numerical simulation in predicting pressure and production behavior for a horizontal well with multiple transverse fractures under constant rate and constant bottomhole flowing pressure operating conditions.
- To apply the method as an optimization tool to obtain optimum design parameters, including optimum dimension and spacing of fracture "stages".
- To apply the method to forecast and analyze the pressure and productivity behavior of a state-of-the-art horizontal completion in the tight oil Bakken formation.

1.4 Organization of the Thesis

The outline of the thesis is as follows:

- Chapter I — Introduction
  - Statement of the Problem
  - Literature Review
  - Research Objective and Approach
- Chapter II — Model Development and Validation
  - Productivity Index
  - Development of Numerical Model
  - The Concept of Proppant Number
  - Model Validation

CHAPTER II

MODEL DEVELOPMENT AND VALIDATION

2.1 Productivity Index

The productivity index (J) represents the ratio of production rate to the pressure difference between the reservoir and the well. The productivity index will be time invariant once the system reaches a stabilized condition under an operating condition. Usually two such conditions are considered constant production rate or constant wellbore flowing pressure. The model assumes impermeable boundaries of the rectangular shapes reservoir (or in other words we model a volumetric reservoir). The expression for productivity index is given as

$$J = \frac{q}{(p_{ave} - p_{wf})} \quad \text{.....(2.1)}$$

The flow regime that provides constant productivity under constant rate production is known as pseudosteady-state. For constant bottomhole pressure it is known as boundary dominated-state. Productivity index can be expressed in dimensionless terms as the dimensionless productivity index,

$$J_D = \frac{\mu B}{2\pi kh} J \quad \text{.....(2.2)}$$

Economides *et al.* (2002) pointed out that the PSS (pseudosteady-state) dimensionless productivity index,

$$J_D = function \ \ of \ drainage - volume, \ geometry, \ and \ fracture \ \ parameters \quad \text{.....(2.3)}$$

The transient – pseudosteady-state productivity can be represented as a function of dimensionless time with respect to the drainage area (**Fig. 2.1**), t_{DA}:

$$t_{DA} = \frac{k}{\phi \mu c_{te} (x_e y_e)} t \quad \text{.....(2.4)}$$

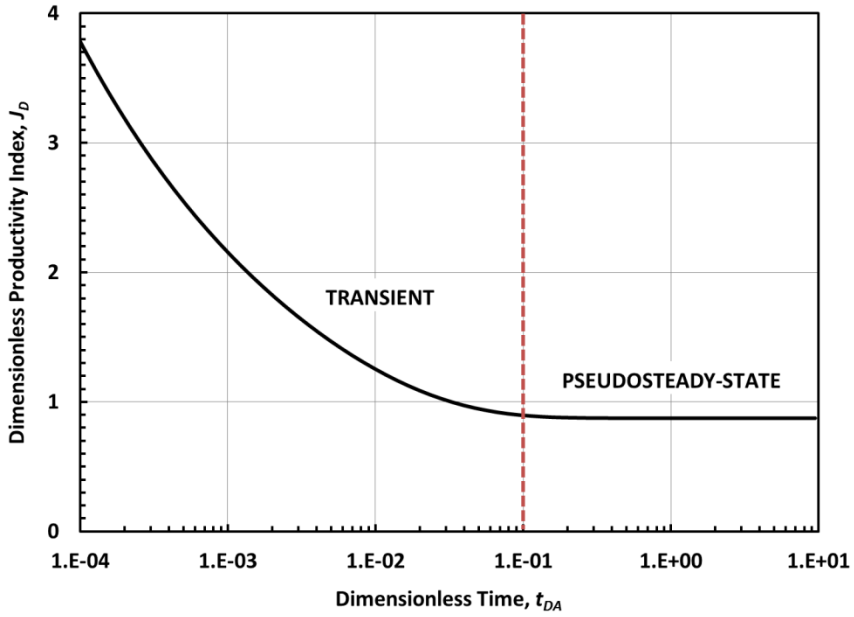

Figure 2.1 — Transient and Pseudosteady-state productivity

Helmy and Wattenbarger (1998) showed that the stabilized productivity index is not unique for different operating conditions. This statement will be investigated also in the next chapter for the case of horizontal well with transverse fractures.

2.2 Development of Numerical Model

Reservoir simulation code is developed and modified specifically for the purposes of this work from TOUGH family of simulation tools for flow and transport processes in porous media (Pruess, 1991). The original code was developed by researchers in Earth Sciences

division of Lawrence Berkeley National Laboratory. An up-to-date version written in FORTRAN 95, is used as a starting point.

The reservoir model might be isotropic or anisotropic with homogeneous reservoir properties and impermeable boundaries. Slightly compressible fluid is used in this simulation model, highly compressible fluid or gas might also be used for future research purposes. Viscosity (μ) for the fluid and total compressibility are assumed to be constant. The expansion of the fluid during reservoir depletion is represented by an exponential function (**Eq. 2.4**).

$$\rho_o = \rho_{ref} \times \exp\left[c_o \times \left(p - p_{ref}\right)\right]. \quad (2.5)$$

Reservoir properties such as porosity and permeability are assumed to be constant during depletion, the gravity effects being neglected. For the fractured well cases, the fluid is produced through the induced fractures with characteristics: fracture half length (x_f), width (w), permeability (k_f), and porosity (ϕ_f), all assumed to be constant during production.

The numerical simulation model assumes that uniform fractures are created in horizontal wells. However, distinct fractures of varying characteristics can also be modeled in this numerical simulator, and this might be useful for future research. The productivity of each fracture is assumed to be equal, then the total productivity of well-fracture system is the productivity from one single fracture multiplied by the number of fractures as shown in **Eq. 2.5**:

$$J_{D,Total} = n_{frac} \times J_D \,. \quad (2.6)$$

Appendix A shows the concepts, underlying physics, and the details of the governing equations implemented in the numerical simulator.

2.3 The Concept of Proppant Number

The performance of a fractured vertical well is known to be determined by the lateral penetration ratio and also by the dimensionless fracture conductivity:

$$I_x = \frac{2x_f}{x_e}. \quad (2.7)$$

$$C_{fD} = \frac{k_f w}{k x_f} \quad (2.8)$$

Valko and Economides (2002) introduced the optimization technique to maximize the productivity of hydraulically fractured well for a square reservoir, introduced the dimensionless proppant number:

$$N_{prop} = I_x^2 C_{fD} = \frac{4k_f x_f w}{k x_e^2} = \frac{4k_f x_f wh}{k x_e^2 h} = \frac{2k_f}{k}\frac{V_{prop}}{V_{res}} \quad (2.9)$$

where N_{prop} is the dimensionless proppant number; k_f is the effective proppant pack permeability, k is the formation permeability, V_{prop} is the propped fracture volume for two fracture wings, and V_{res} is the reservoir drainage volume. For the reservoir that is not square shape ($x_e \neq y_e$), the proppant number will be

$$N_{prop} = \frac{2k_f}{k}\frac{V_{prop}}{V_{res}} = \frac{2k_f}{k}\frac{2x_f wh}{x_e y_e h} = \frac{1}{A_r} I_x^2 C_{fD}. \quad (2.10)$$

where the aspect ratio, $A_r = x_e / y_e$. We emphasize that volumetric definition of the proppant number remains valid for the general case, when the fracture is not fully penetrating vertically.

2.4 Model Validation

Many researches have been conducted and there are no exact solutions for the complex problems being studied in this work. However, the model in this work can be validated and verified by using sample solutions of the simpler problems. Here the numerical model is verified by comparing it to the analytical solutions, calculation of Dietz shape factor (Dietz, 1965), and productivity of fractured vertical well calculated by the boundary element method (Romero and Valko, 2003).

Durlofsky (1991) showed that the average reservoir pressure can be computed with pressure weighted by a basis function which in this study will be porosity or element volume (**Eq. 2.9**). This method of calculation is compared with the average reservoir pressure calculated from material balance (**Eq. 2.10**) if the total effective compressibility, c_{te}, can be considered constant.

$$p_{ave} = \sum_{n=1}^{NumElem} p_n \times \frac{V_n}{V_{total}} \quad \text{.....(2.9)}$$

$$p_{ave} = p_i - \frac{Np}{c_{te} \times N} \quad \text{.....(2.10)}$$

2.4.1 Fully Penetrating Vertical Well (Radial Flow Solution)

The assumption that the fractured well will drain a rectangular drainage area is used for this study. However, the well-known analytical solution for radial flow might be useful as a basis of comparison for both single phase oil and gas flow in order to validate the numerical model. The solution of radial flow for vertical well producing under constant rate in a bounded cylindrical reservoir in Laplace space can be written as **Eq. 2.11**.

$$\overline{p_D}(r_{eD}, r_D, u) = \frac{1}{u} \frac{K_1(\sqrt{u}\, r_{eD}) I_0(\sqrt{u}\, r_D) + I_1(\sqrt{u}\, r_{eD}) K_0(\sqrt{u}\, r_D)}{\sqrt{u}\left[K_1(\sqrt{u}\,) I_1(\sqrt{u}\, r_{eD}) - I_1(\sqrt{u}\,) K_1(\sqrt{u}\, r_{eD})\right]} \quad \text{.....(2.11)}$$

where,

$r_{eD} = \frac{r_e}{r_w}$

$r_D = \frac{r}{r_w}$

$I_0 =$ zero order modified Bessel function of the first kind

$I_1 =$ first order modified Bessel function of the first kind

$K_0 =$ zero order modified Bessel function of the second kind

$K_1 =$ first order modified Bessel function of the second kind

Equation 2.11 can be numerically inverted to obtain the solution which is the dimensionless pressure, p_D, where

$$p_D = \frac{2\pi kh}{qB\mu}(p_i - p_{ave}). \quad \text{.....(2.12)}$$

For the comparison, we used a one-dimensional radial mesh with the properties shown in **Table 2.1**.

Table 2.1 – Model parameters for analytic solution match, cylindrical reservoir

k	=	250 md	p_i	=	3626 psi
ϕ	=	0.25	c_t	=	1.38×10^{-5} 1/psi
h	=	59 ft	r_e	=	3281 ft

Figures 2.2 and **2.3** show the good agreement between analytical and numerical solutions for single phase oil and gas respectively, producing under constant rate operating conditions. The comparisons are shown in the pressure and dimensionless pressure terms. The maximum error was 4% and occurred near the wellbore.

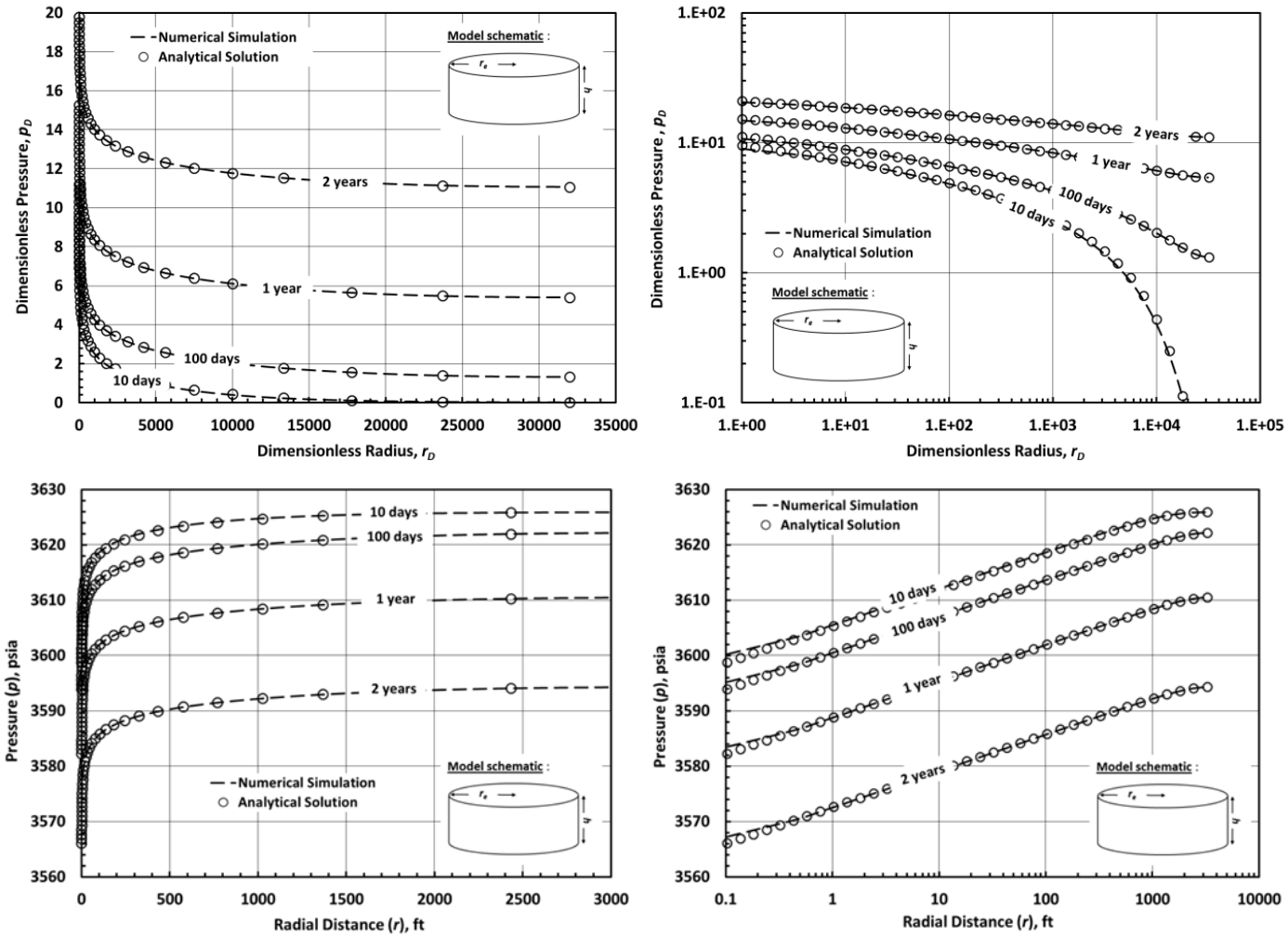

Figure 2.2 — Comparison of the Simulation Result with Analytical Solution: Vertical Well in a Bounded Cylindrical Reservoir, Single Phase Oil

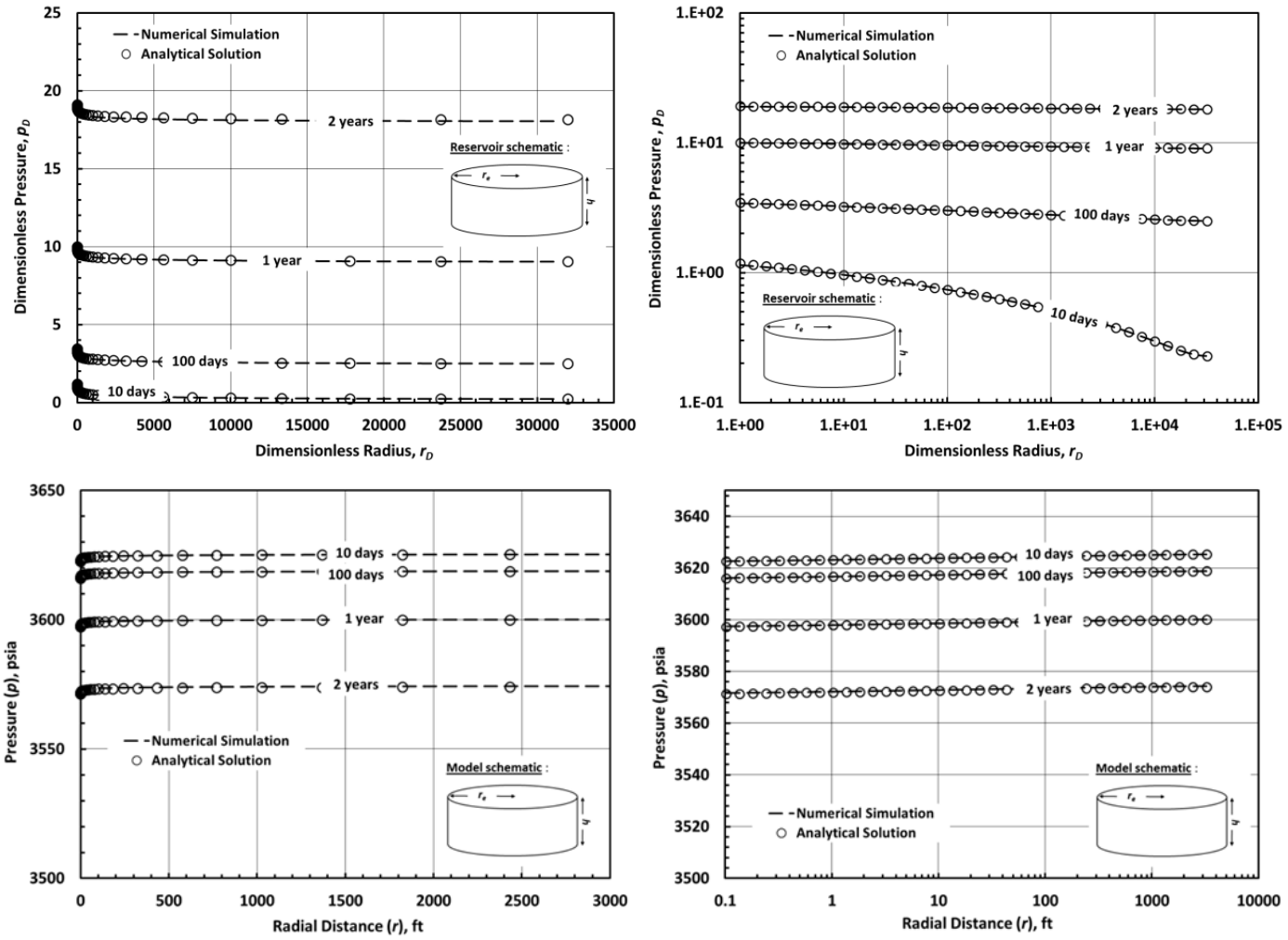

Figure 2.3 — Comparison of the Simulation Result with Analytical Solution: Vertical Well in a Bounded Cylindrical Reservoir, Single Phase Gas

2.4.2 Recalculation of Dietz Shape Factor

Dietz (1965) has shown that particular drainage area shape and well position will affect the well performance in such a way, that can be characterized by a dimensionless parameter termed "shape factor", C_A. Dimensionless productivity index for various shape factors can be formulated as

$$J_D = \frac{1}{\frac{1}{2}\ln\frac{4A}{e^{\gamma}c_A r_w^2} + s} \quad \text{.....(2.13)}$$

Fully penetrating vertical well producing under constant rate in a square drainage area is used to reproduce the Dietz shape factors by our simulator. **Figure 2.4** shows the logarithmic increasing gridblock size ("logarithmic mesh") that will be used throughout this study.

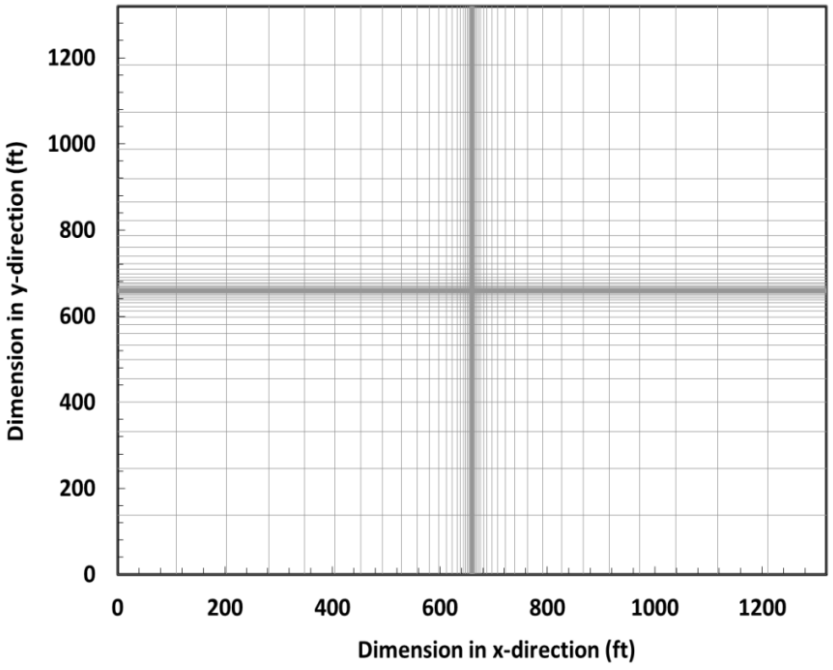

Figure 2.4 — Logarithmic Mesh

Detailed numerical experimentation indicated that the equivalent wellbore radius for this model is as follow:

$$x_0 = 0.4 \times r_w . \quad (2.14)$$

where x_0 is the gridblock size where the well is located. For the case of horizontal well, $z_0 = x_0$ and for vertical well, $y_0 = x_0$.

First of all, we specified the size of the gridblock where the well is located, x_0. The dimensionless productivity index and shape factor, C_A, are calculated for each given x_0. The equivalent wellbore radius is calculated by solving the **Eq. 2.13** with dimensionless productivity index as the known variable. **Table 2.2** shows detailed result of numerical experimentation to determine equivalent wellbore radius.

Table 2.2 Detailed numerical experiment to determine equivalent wellbore radius

x_0, ft	$r_w = 0.4\,x_0$, ft	J_D (simulation)	J_D (Eq. 2.13)	C_A (simulation)	C_A (Dietz, 1965)
0.1	0.04	0.110	0.110	31.056	30.881
0.2	0.08	0.119	0.119	30.710	30.881
0.3	0.12	0.125	0.125	30.581	30.881
0.4	0.16	0.130	0.130	31.830	30.881
0.5	0.20	0.134	0.134	32.245	30.881

The dimensionless productivity indices calculated by numerical simulation are in a good agreement up to three decimal places compared to the results calculated by **Eq. 2.13**. However, the calculated shape factors are quite different with the maximum error of 4.5%. It is also shown from the table that the difference between calculated shape factors by simulation and **Eq. 2.13** becomes greater for higher x_0 or r_w.

Figure 2.5 shows the simulated pressure for this case, the pseudosteady-state regime can be recognized when the wellbore flowing pressure and reservoir average pressure are decreasing with the same rate. **Figure 2.6** shows the calculated average reservoir pressure from two methods that already mentioned before, the two methods provide a good agreement with each other, thus any of them can be implemented in the computational procedure.

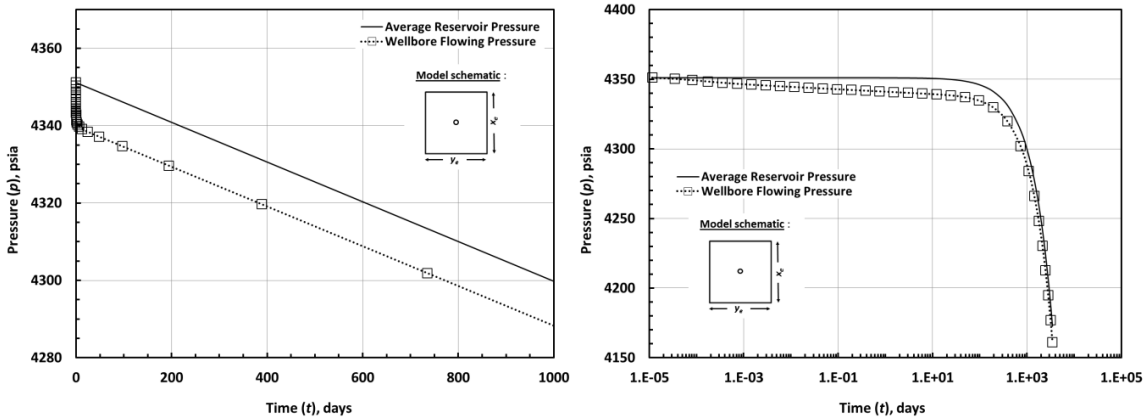

Figure 2.5 — Average Reservoir Pressure and Wellbore Flowing Pressure – Simulation Result

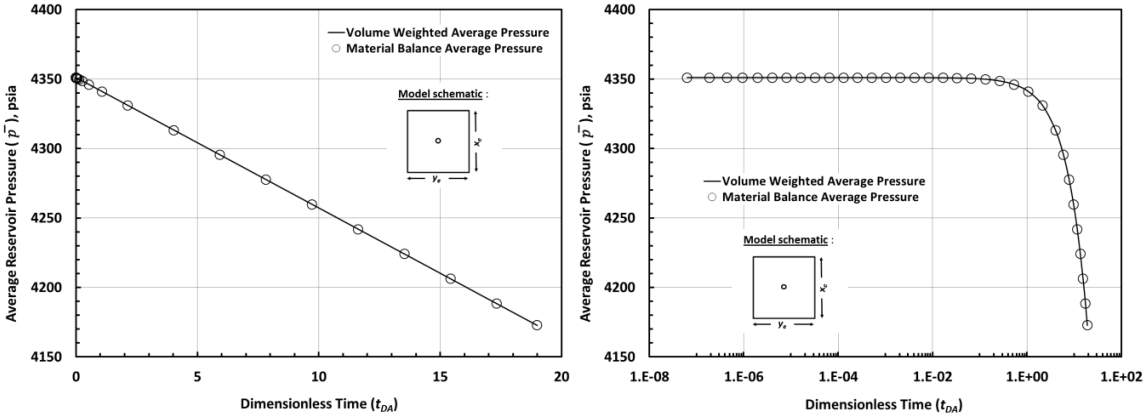

Figure 2.6 — Comparison of the Average Pressure from Material Balance and Pressure Weighted by Elements Volume

2.4.3 Fully Penetrating Finite Conductivity Vertical Fracture

Figure 2.7 represents the behavior of dimensionless productivity index calculated by simulation and boundary element method for the vertical well intersected by fully penetrating vertical fracture with varying fracture characteristics I_x and C_{fD}. Both methods provide consistent results and the largest difference between them occurs at smaller dimensionless fracture conductivity.

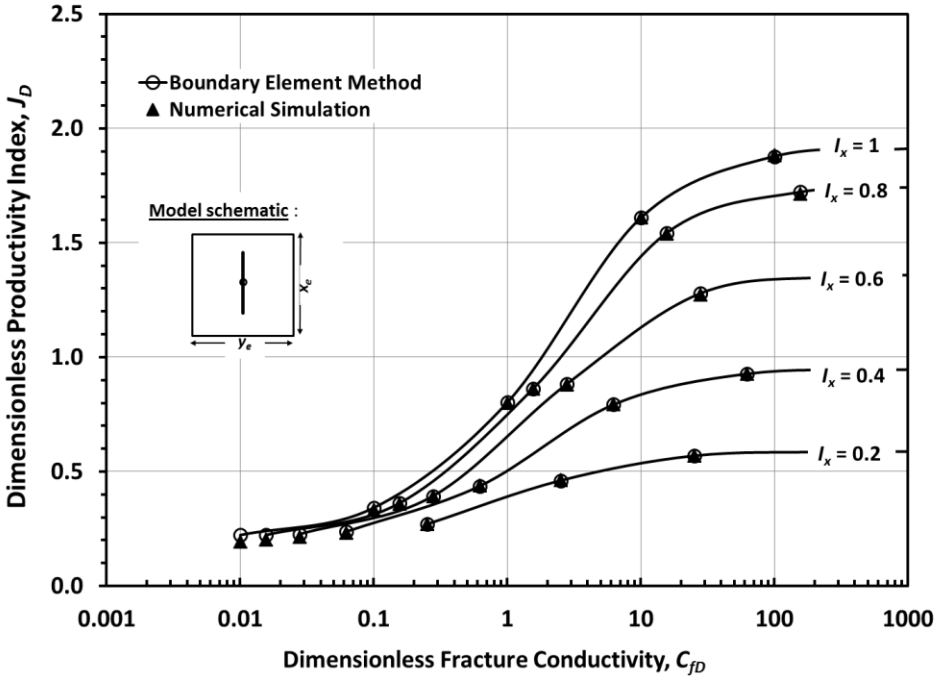

Figure 2.7 — Dimensionless productivity index computed from simulation and boundary element method by Romero and Valko (2003) as a function of C_{fD} with I_x as a parameter, N_{prop} = 1

Figure 2.8 below shows a good agreement between dimensionless productivity index from simulation and boundary element method for various rectangular drainage

areas. "Amount of proppant" is considered constant for all of the cases (N_{prop} = 1), in other words the proppant number was fixed.

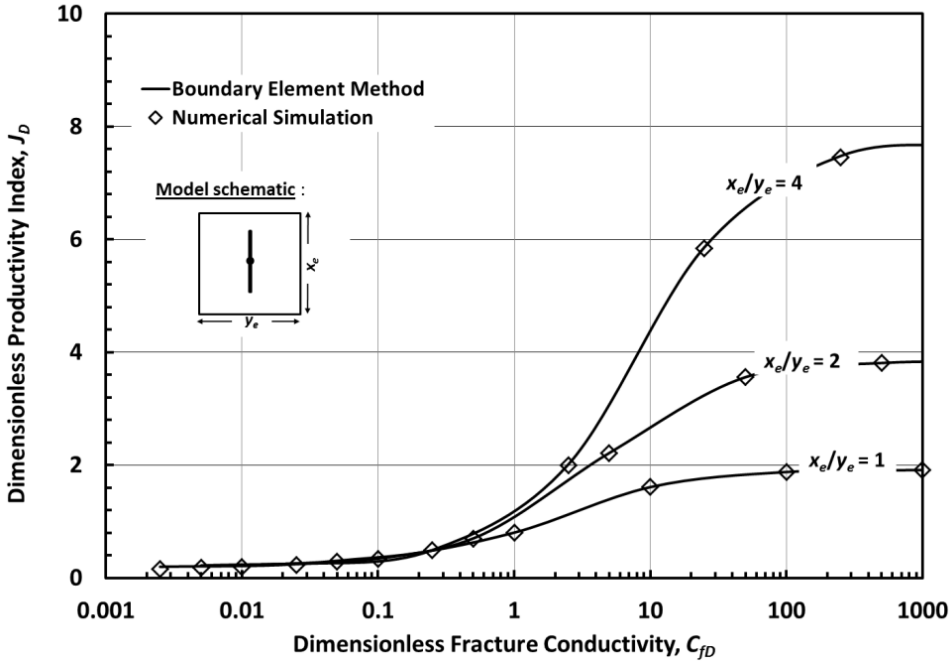

Figure 2.8 — Comparison of the simulated dimensionless productivity index with boundary element method by Romero and Valko (2003) for various aspect ratios, N_{prop} = 1

The productivity of fully penetrating vertical fracture is proportional to aspect ratio (Sabaev *et al.*, 2006). As for a well intersected by infinite conductivity fracture, the dimensionless productivity index is presented as follow:

$$J_D = \frac{6}{\pi} \times A_r \quad \text{.....(2.15)}$$

It can be seen from the figure that **Eq. 2.15** holds true for the cases of very high dimensionless fracture conductivity.

CHAPTER III

NUMERICAL SIMULATION OF FRACTURED WELL

3.1 Choke Skin

As mentioned before, the existence of additional pressure drop due to flow convergence (limited contact area) is causing productivity reduction in the case of horizontal well – transverse fractures. This additional pressure drop can be represented by an appropriate skin factor which will be called choke skin factor. Mukherjee and Economides (1991) derived the expression to calculate the choke skin as follows

$$s_c = \left(\frac{kh}{k_f w}\right)\left[\ln\left(\frac{h}{2r_w}\right) - \frac{\pi}{2}\right]. \quad \text{.....(3.1)}$$

Equation 3.1 above shows that the choke skin depends heavily on the ratio of height to wellbore radius.

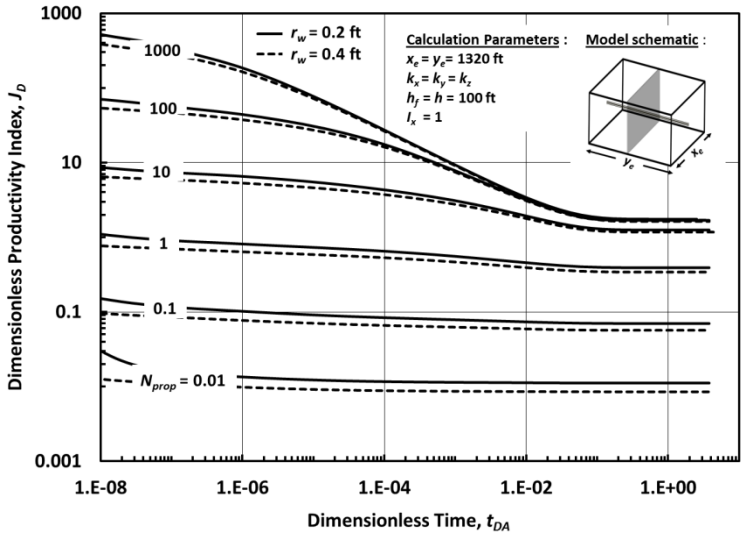

Figure 3.1 — Transient and pseudosteady-state productivity of horizontal well with transverse fracture with r_w = 0.2 ft and r_w = 0.4 ft for various N_{prop}

As shown on **Fig. 3.1**, for smaller proppant number, the smaller wellbore radius gives more productivity penalty and this effect starts to disappear especially for the stabilized productivity regime when the proppant number is large enough.

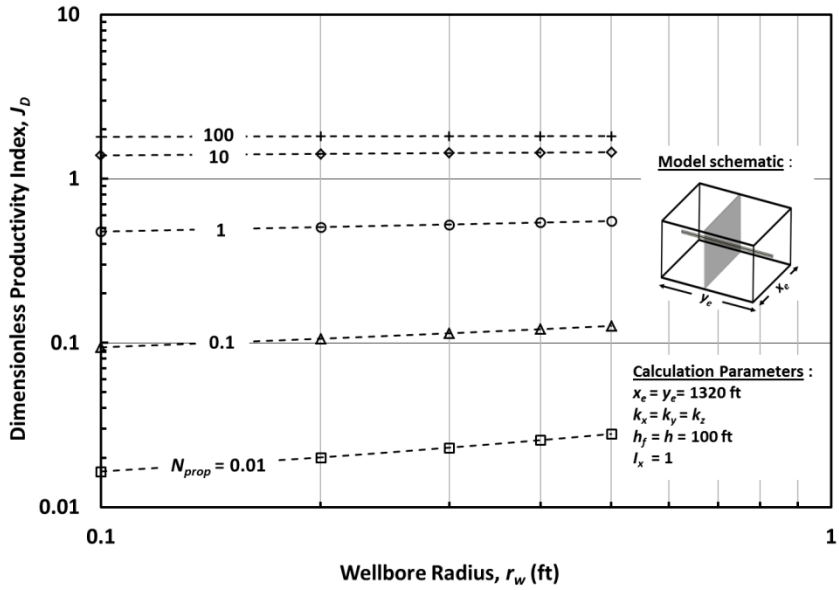

Figure 3.2 — Pseudosteady-state productivity for horizontal well with transverse fracture with various N_{prop} and r_w

The productivity depends significantly on the wellbore radius for very small proppant numbers, as shown in **Fig 3.2**.

However, minimizing the choke skin effect by increasing the wellbore radius is not the best approach since there exist more important constraints for choosing the appropriate wellbore radius; the typical wellbore radius is between 0.2 – 0.7 ft. The proppant number in tight formation also becomes larger because of the great permeability contrast between proppant and formation, thus increasing wellbore radius

will not result in huge improvement to the productivity. In general, it is more straight forward to realize a sufficient large proppant number. The productivity penalty becomes very small for the system with infinite-conductivity fracture as shown in **Fig. 3.3**.

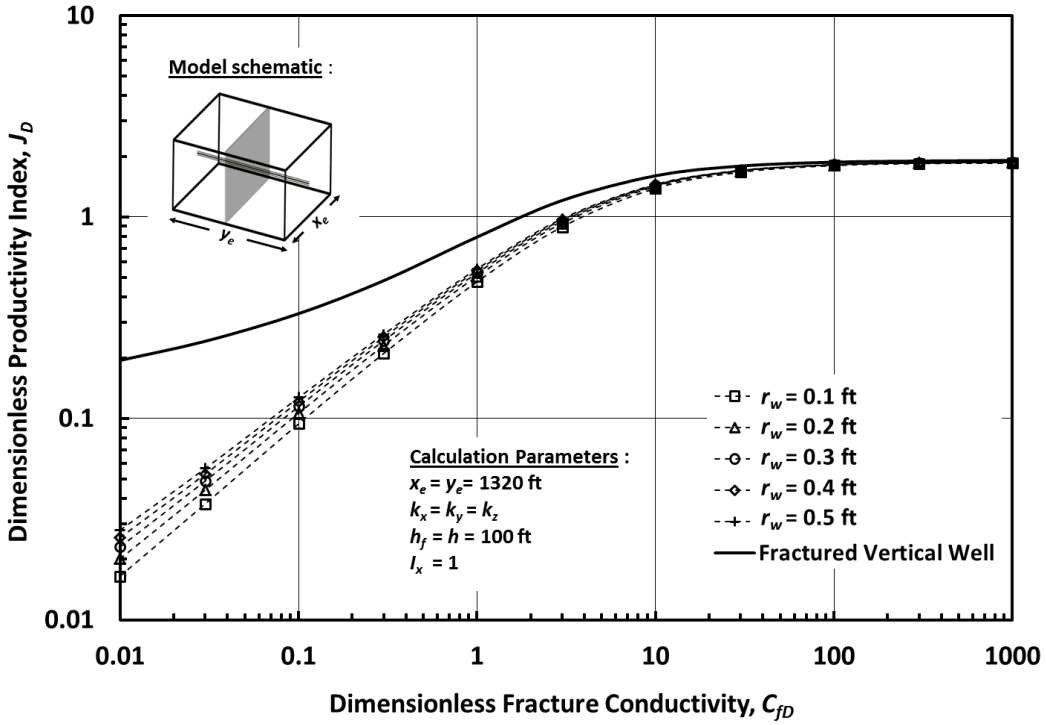

Figure 3.3 — Pseudosteady-state productivity for horizontal well with transverse fracture and fractured vertical well as a function of C_{fD} with various r_w

It is shown in **Fig. 3.4** that the choke skins calculated by **Eq. 3.1** and from the simulations are in a good agreement. It is expected that the computation results indicate very small differences for higher fracture conductivity or for infinite-conductivity fracture.

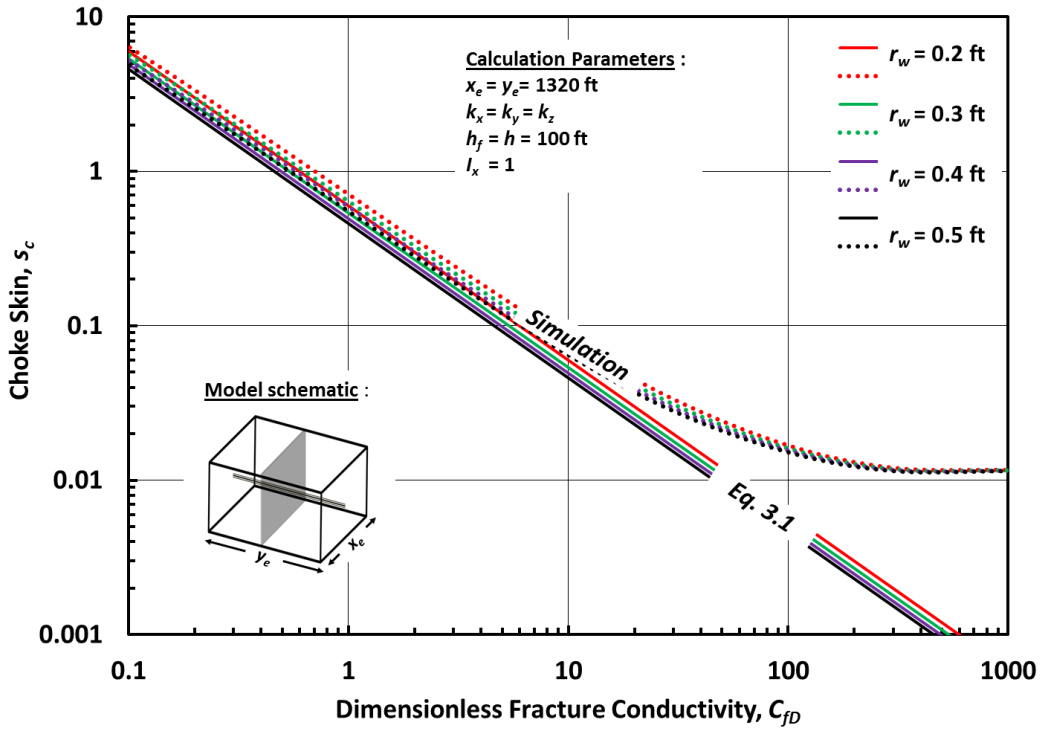

Figure 3.4 — Choke skin for various r_w as a function of C_{fD}

3.2 Productivity of Hydraulically Fractured Well

Economides *et al.* (2002) appointed that there is a unique maximum productivity for each given proppant number (N_{prop}). The optimum dimensionless fracture conductivity (C_{fD}) is always 1.6 for proppant numbers less than 0.1; on the other hand, the optimum C_{fD} for larger proppant numbers occurs at larger dimensionless fracture conductivities.

Figures 3.5 and **3.6** show the dimensionless productivity as a function of dimensionless fracture conductivity for the case of vertical well intersected by fully penetrating vertical well with proppant numbers less than 0.1 and more than 0.1 respectively.

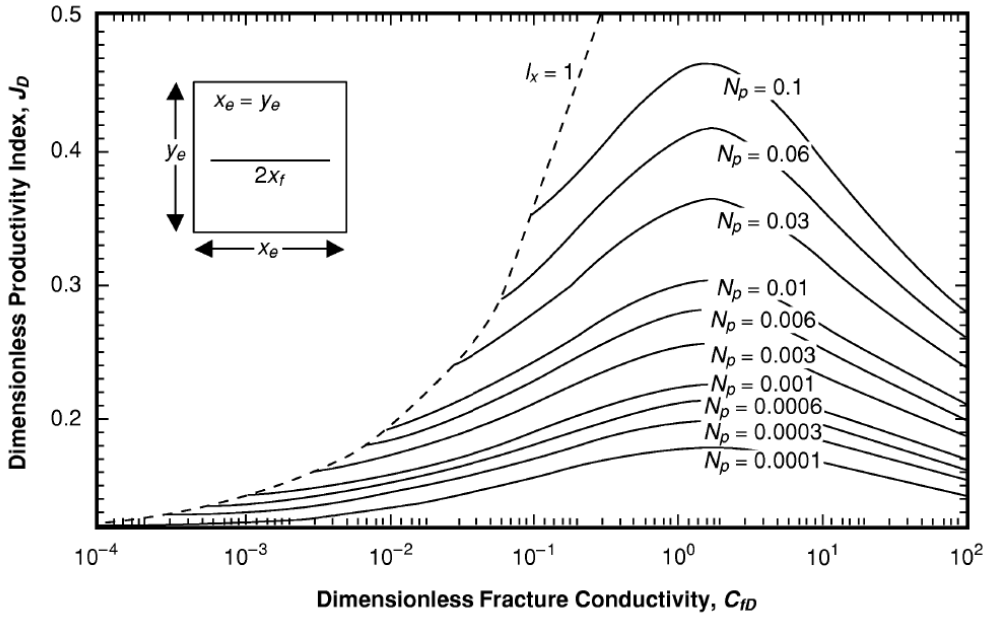

Figure 3.5 — Dimensionless productivity index of a fully penetrated vertical fracture as a function of dimensionless fracture conductivity, with proppant number as a parameter for N_{prop} < 0.1 (Economides *et al.* 2002)

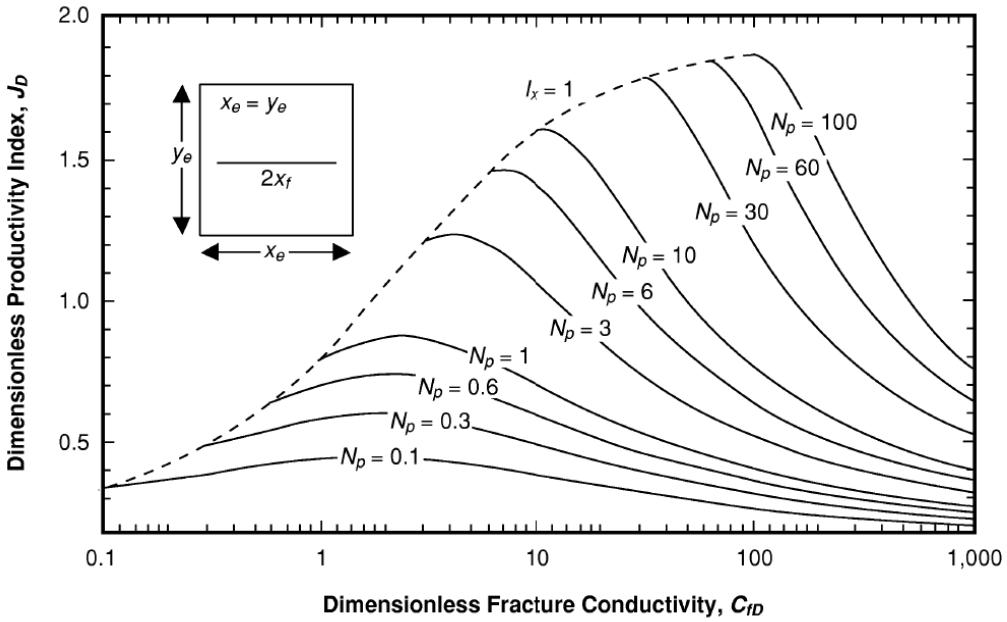

Figure 3.6 — Dimensionless productivity index of a fully penetrated vertical fracture as a function of dimensionless fracture conductivity, with proppant number as a parameter for N_{prop} > 0.1 (Economides *et al.* 2002)

The maximum dimensionless productivity of vertical well intersected by fully penetrating vertical fracture is well known to be 6/π (Wattenbarger, 1998), this corresponds to perfect linear flow in the reservoir.

Numbers of simulation for horizontal well with transverse fracture are conducted to investigate the behavior of productivity as a function of dimensionless fracture conductivity with proppant number as a parameter.

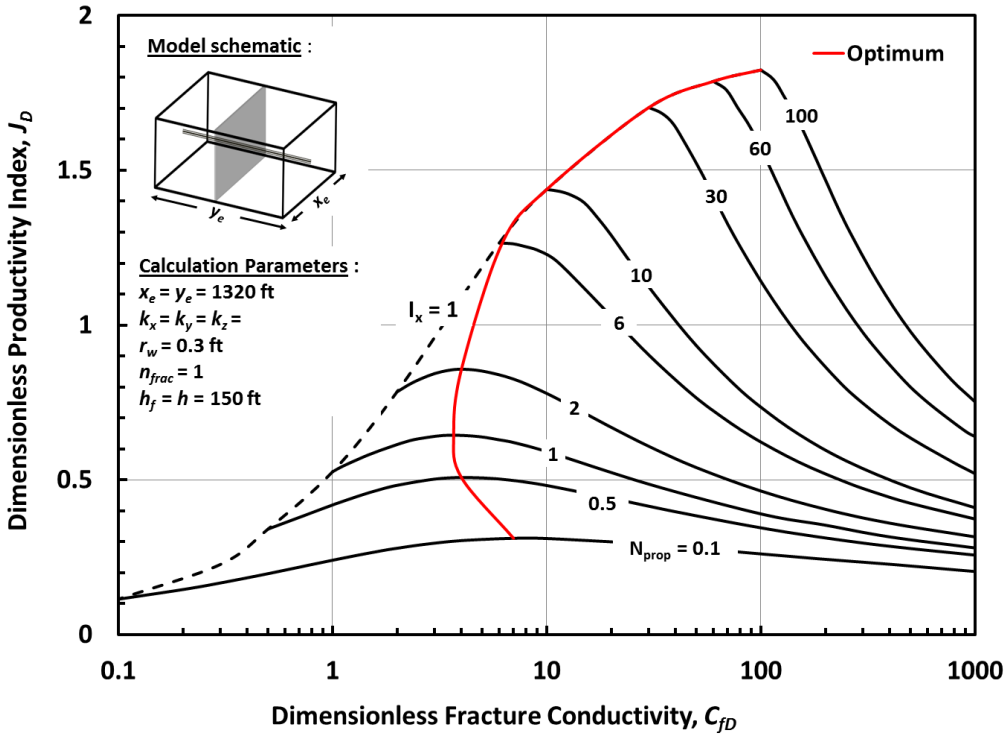

Figure 3.7— Dimensionless productivity index of a horizontal well intersected by single transverse fracture as a function of C_{fD}, with N_{prop} as a parameter

Figure 3.7 shows the stabilized productivity as a function of dimensionless fracture conductivity with proppant number as parameter for the case of horizontal well

intersected by a transverse fracture. It can be seen that the optimum dimensionless conductivity for proppant number equal to 0.1 is not approaching the value of 1.6 but approaching the larger number (C_{fD} = 7). In the other words, for a particular proppant number, dimensionless fracture conductivity for the transverse fracture that intersects horizontal well needs to be large enough to approach the maximum productivity compared to the fractured vertical well case. The dimensionless productivity indices for this proppant number also being penalized by more than 30% compared to the fractured vertical well. This phenomenon describes how the choking of flow around the wellbore affecting the productivity of the well-fracture system, especially for smaller proppant numbers.

Table 3.1 below shows the optimum C_{fD} that gives the maximum productivity for each given proppant number for fractured vertical well and horizontal well with transverse fracture.

Table 3.1 Optimum C_{fD} and maximum J_D for various proppant number

N_{prop}	*Fractured Vertical Well*		*Horizontal Well Transverse Fracture*	
	$C_{fD,opt}$	$J_{D,max}$	$C_{fD,opt}$	$J_{D,max}$
100	100	1.88	100	1.82
60	60	1.85	60	1.79
30	30	1.79	30	1.70
10	11.3	1.61	10	1.44
6	6.9	1.48	6	1.26
2	3	1.10	4	0.86
1	2.3	0.88	3.7	0.64
0.5	2	0.71	4	0.51
1	1.6	0.47	7	0.31
0.05	1.6	0.40	14	0.26

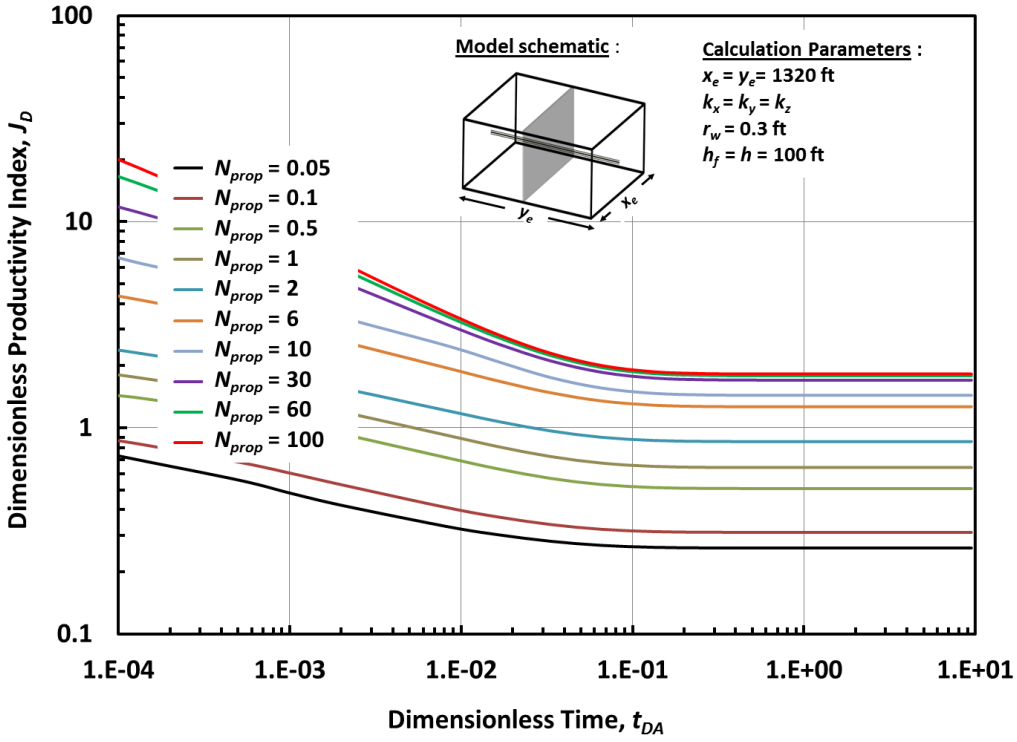

Figure 3.8 — Transient and pseudosteady-state productivity at optimum C_{fD} for various proppant numbers

The transient and pseudosteady-state productivity at optimum C_{fD} for each given proppant number is shown in **Fig. 3.8** above. The figure shows the unique characteristic of the solution: for various proppant numbers, the transient – pseudosteady-state productivity curves (as a function of time) are not crossing each other. This means that the optimum dimensions determined from the optimization of the pseudosteady-state productivity will yield satisfactory conductivity during the transient flow regimes as well. Detailed results of calculated productivity for horizontal well with transverse fracture, productivity trend as a function of C_{fD} for fully penetrating vertical fracture

with various aspect ratios, the effect of partial penetration, and the comparison between vertical and horizontal well cases are shown in the **Appendix B**.

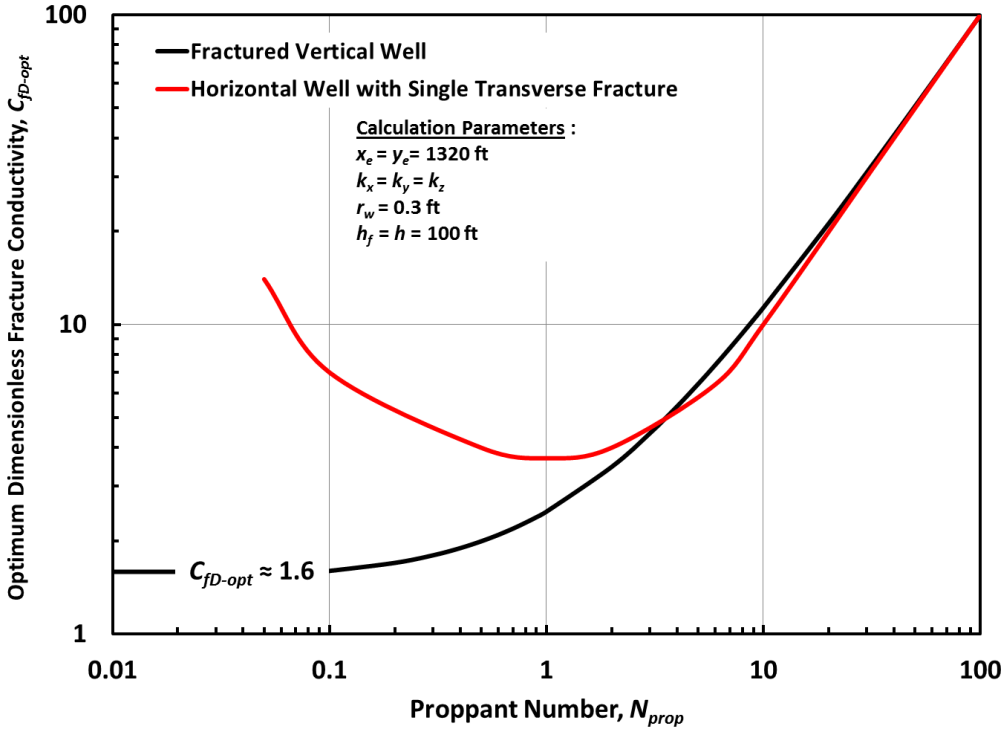

Figure 3.9 — Optimum dimensionless fracture conductivity as a function of N_{prop} for fractured vertical well and horizontal well with a transverse fracture

As mentioned before the optimum dimensionless fracture conductivity is equal to 1.6 for proppant numbers less than 0.1 in the case of fully penetrating vertical fracture intersecting a vertical well. From **Fig. 3.9**, we see that for horizontal well with transverse fracture, the trend of optimum dimensionless fracture conductivity as a function of proppant number is quite different; especially for proppant numbers less than 1.

There is an optimum fracture penetration ratio (I_x) for each given proppant number. **Figure 3.10** shows the the optimum I_x for fractured vertical well and horizontal well with transverse fracture. Based on the observations above, it can be concluded that the fractures should be shorter or wider in order to achieve the optimum productivity in the case of horizontal well compared to the vertical well.

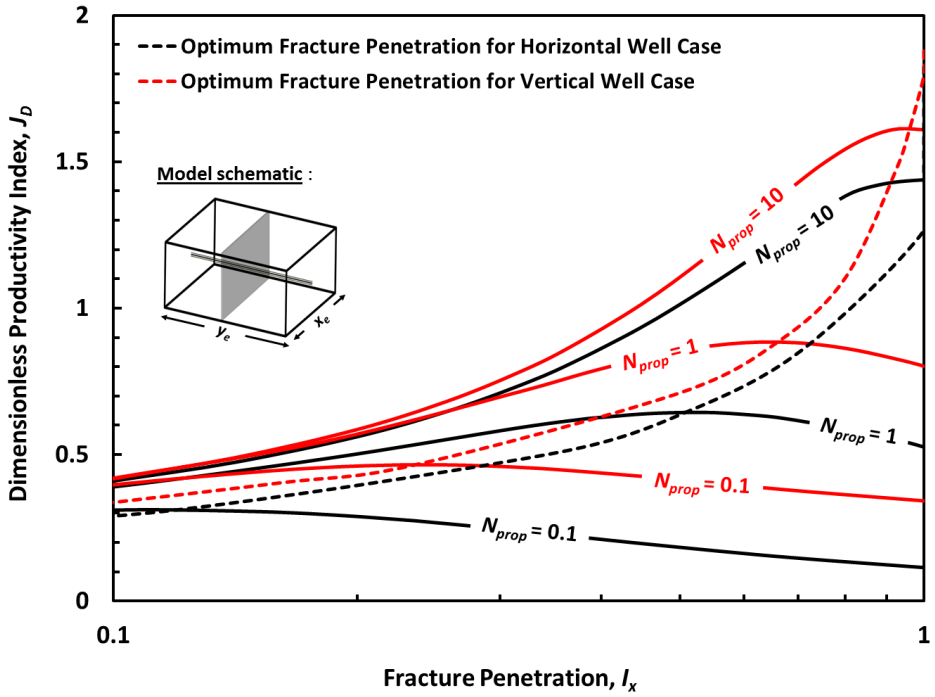

Figure 3.10 — Optimum I_x for fractured vertical well and horizontal well with single transverse fracture

3.3 Flow Distribution of a Transverse Fracture

The flow distribution along the lateral fracture length will reach a stabilized condition shortly after pseudosteady-state conditions are established. It means the relative fluxes

from the reservoir to the fracture at different points on the fracture surfaces will remain the same. This flow distribution will be depending on the fracture characteristics.

Figures 3.11, **3.12**, and **3.13** show the dimensionless source strength distribution along the fracture (half-length) for different proppant number and dimensionless fracture conductivity. Source strengths in the figures are the summation of relative flux from multiple layers who have the same *x*-coordinate. The flux at the tip of the fracture is smaller compared to the flux near the wellbore. This situation is characteristic for C_{fD} less than optimum. The flux at the fracture tip will be larger for higher C_{fD}.

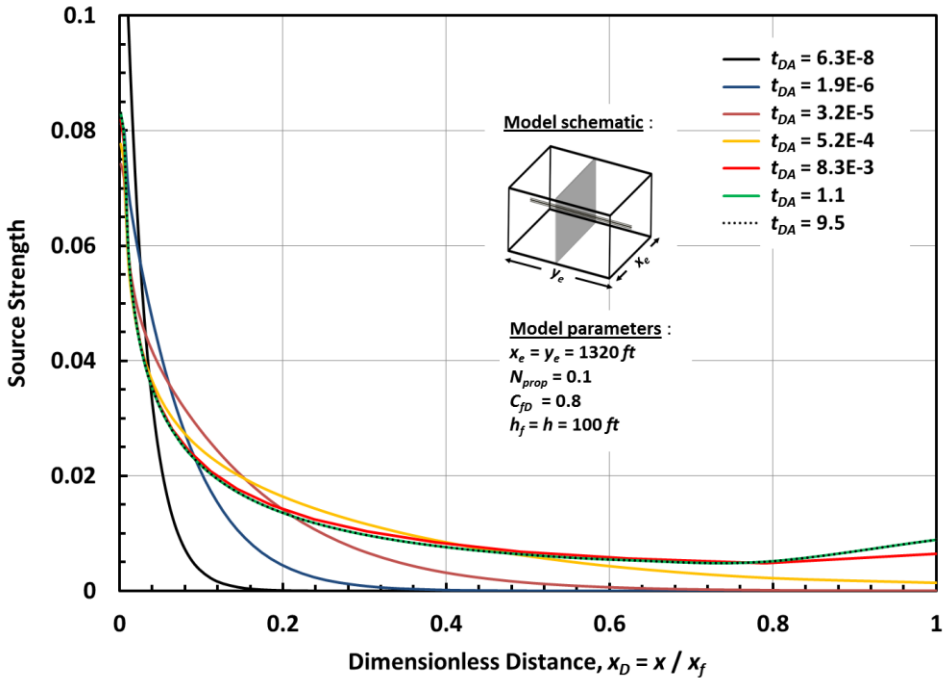

Figure 3.11 — Source strength distribution for a transverse fracture with N_{prop} = 0.1 and C_{fD} = 0.8

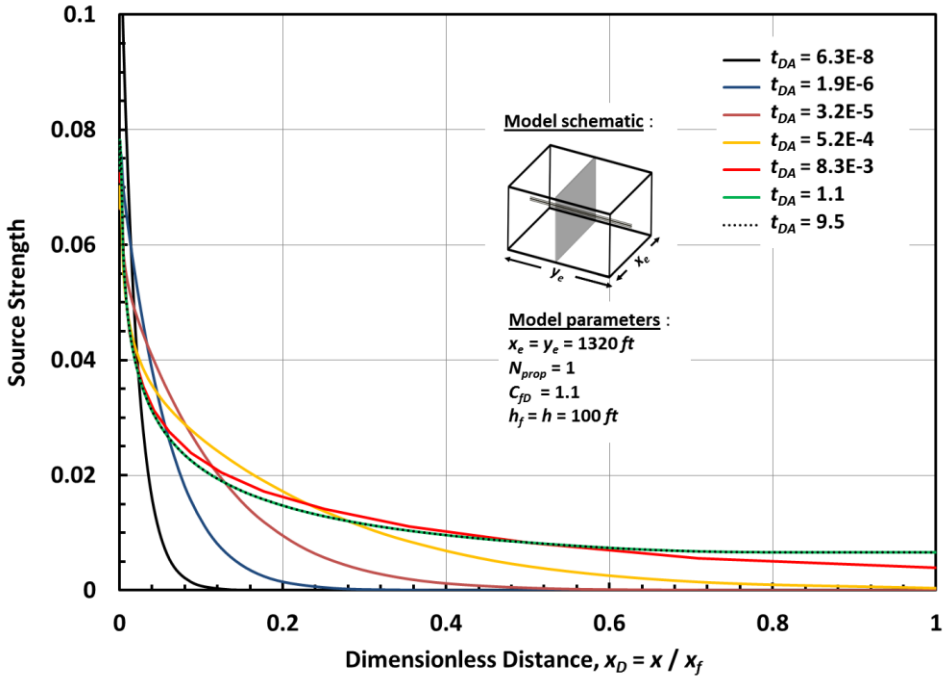

Figure 3.12 — Source strength distribution for a transverse fracture with N_{prop} = 1 and C_{fD} = 1

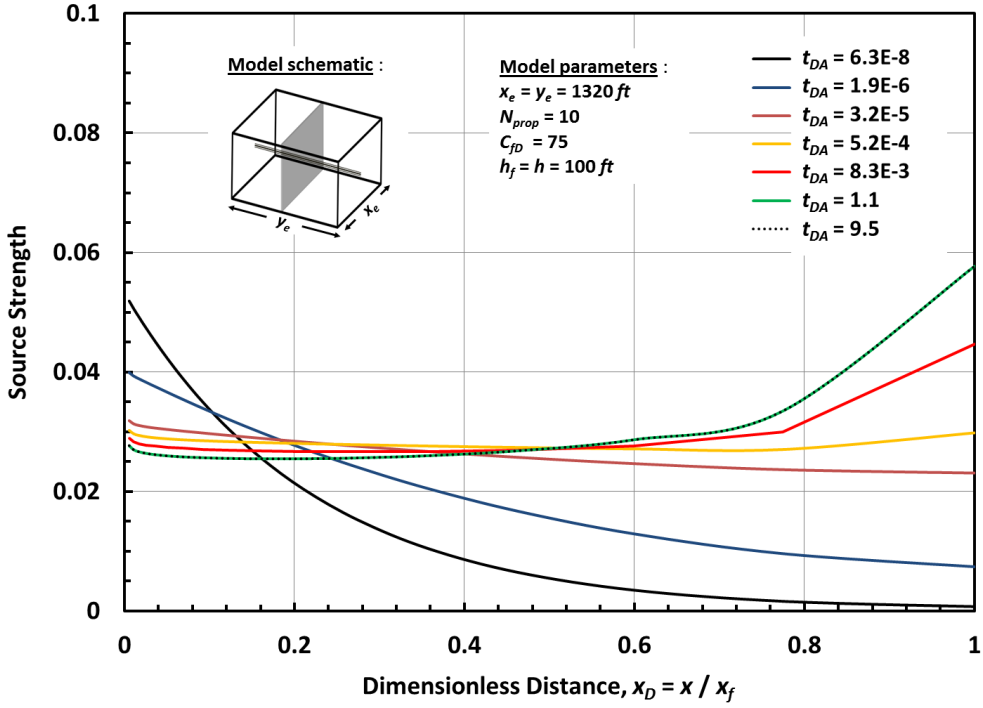

Figure 3.13 — Source strength distribution for a transverse fracture with N_{prop} = 10 and C_{fD} = 75

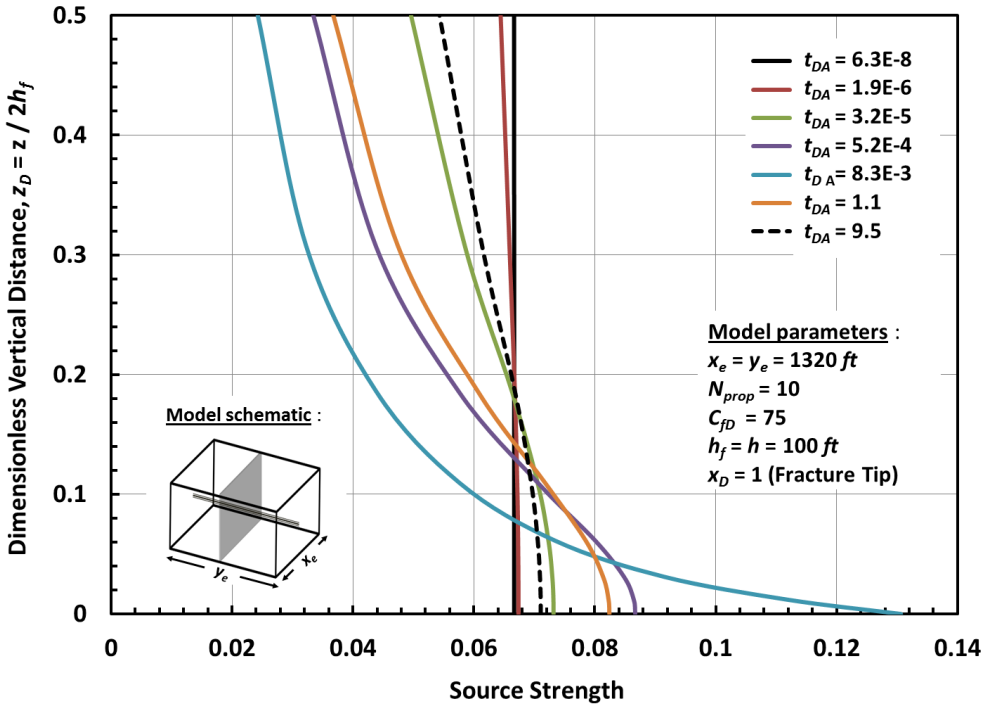

Figure 3.14 — Source strength distribution along *z*-coordinate for a transverse fracture with N_{prop} = 10 and C_{fD} = 75 for various t_{DA} at x_D = 1

Figure 3.14 shows the relative flux distribution along the fracture height at the fracture tip for various times. It can be seen from the figure that the relative flux distributions along the fracture height is not stabilized after the system reaches pseudosteady-state. However, it is notable from the previous figures, the stabilized flux along the fracture length holds true for pseudosteady-state flow regime.

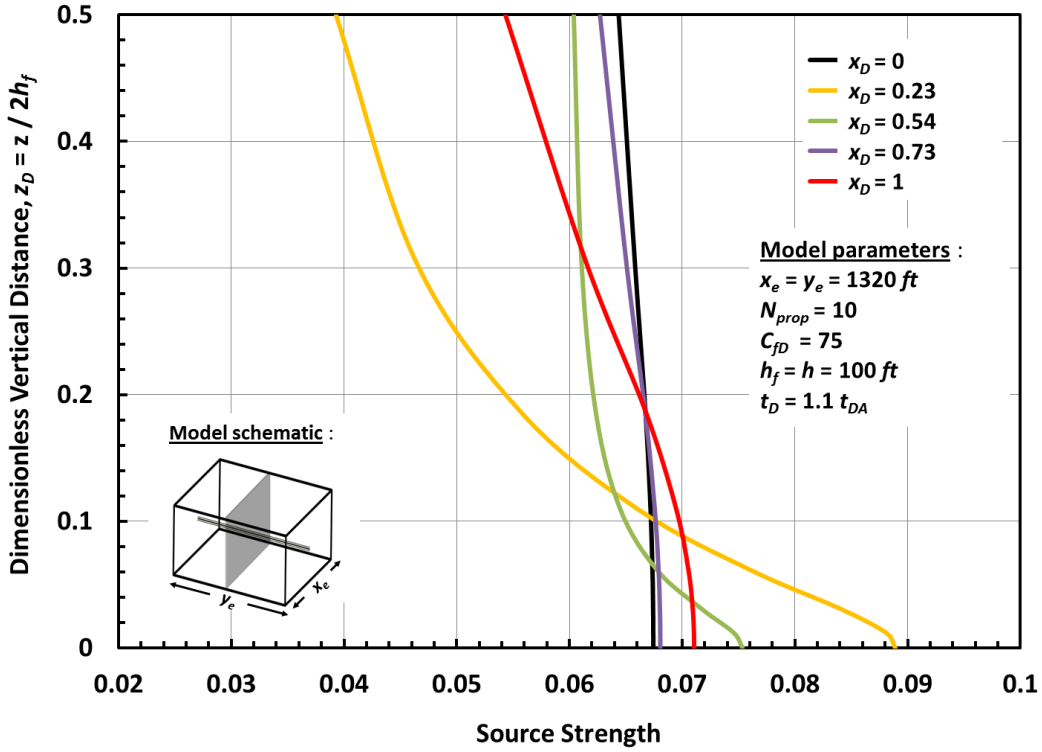

Figure 3.15 — Source strength distribution along *z*-coordinate for a transverse fracture with N_{prop} = 10 and C_{fD} = 75 at various x_D with t_{DA} = 1.1

Figure 3.15 shows the relative flux distribution along the fracture height at various *x*-positions with t_{DA} equal to 1.1. We can see that more flows from reservoir are entering the middle layers compared to the top and bottom layers of the fracture.

3.4 Fracture Design and Optimization

Case of $h_f \neq h$

In this section, we apply the numerical simulation procedures to produce an optimum fracture design for a particular amount of proppant. First of all, the proppant number is considered constant which means the amount or volume of proppant will remains the same. The fracture height might be assumed not equal to the pay thickness. The ratio of

vertical to horizontal permeability of the reservoir will be assumed in the range of 0.01 to 1.

The productivity in the reservoir that has higher vertical permeability is expected to be greater than the others that have lower vertical permeability especially for the case when the fracture does not fully penetrate along the formation thickness. Of course, there are no guarantee that the fracture will always cover the pay thickness. **Table 3.2** shows the detail of the parameters that will be used for this example case.

Table 3.2 – Model parameters for optimization example

k_x	$= k_y$	$=$ 1 md
k_z		$=$ 1 md, 0.1 md, 0.01 md
k_f		$=$ 10,000 md
ϕ_f	$= \phi$	$=$ 0.1
w		$=$ 0.016 – 0.1 ft
h		$=$ 100 ft
r_w		$=$ 0.3 ft
N_{prop}		$=$ 1
c_t		$=$ 1.4×10^{-5} psi^{-1}

The number of fractures that will be examined in this example case will be 1, 2, and 4 fractures. The reservoir volume and dimension will remain the same as the previous part of this study which is 1320 ft × 1320 ft × 100 ft, and as mentioned earlier, the productivity of the total fractures system will be the productivity of one fracture multiplied by the number of fractures. Note that for number of fractures more than 1, each fracture can be assumed to have its own drainage area or reservoir dimension which is identical with the other fractures. **Figure 3.16** shows the illustration of this condition.

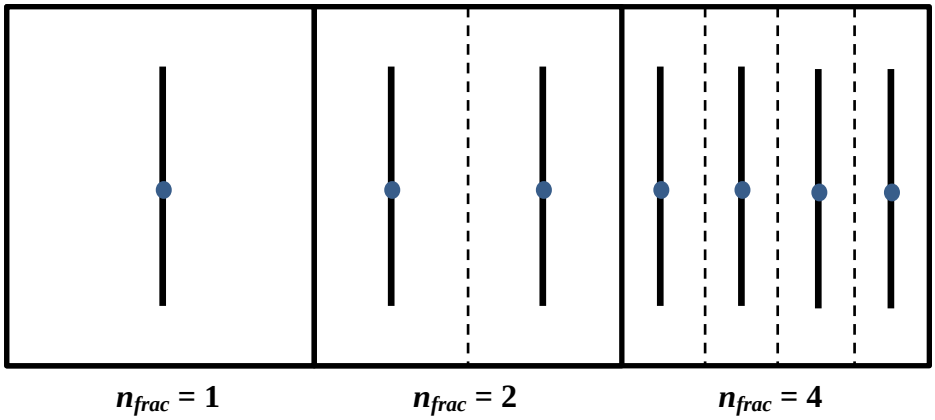

Figure 3.16— Model schematic of multiple fractures system

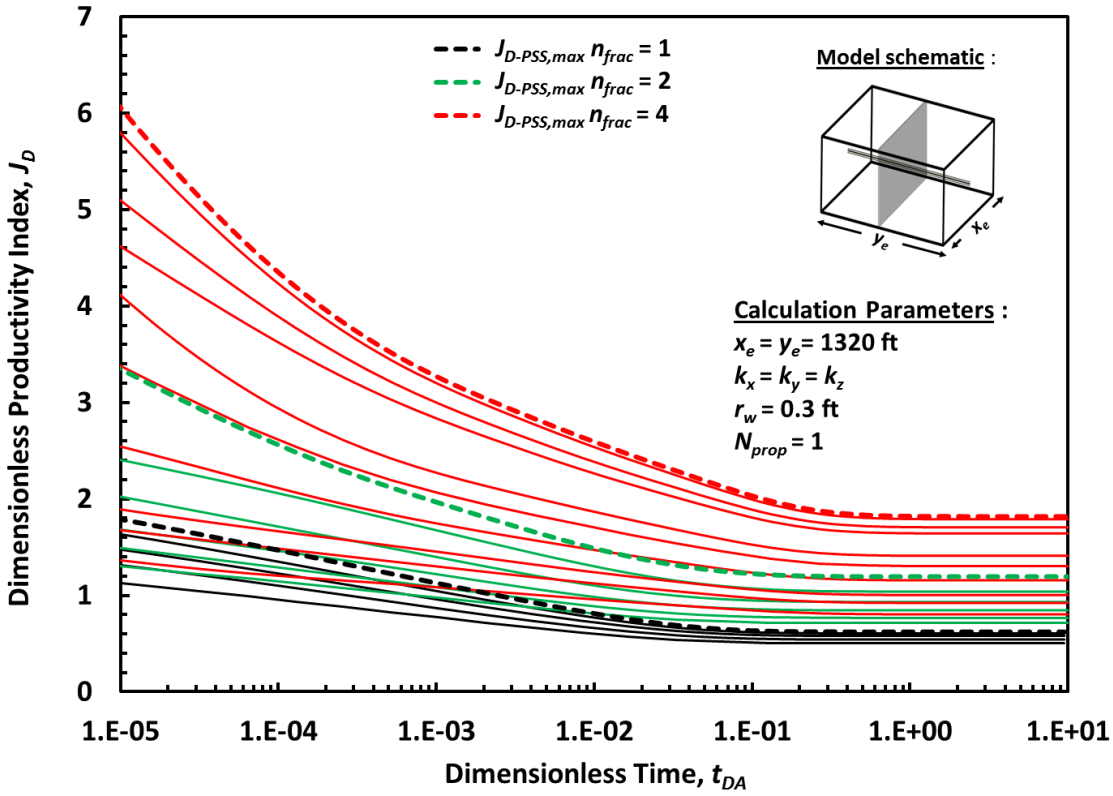

Figure 3.17— Transient and pseudosteady-state productivity for example case

The transient and pseudosteady-state productivity is shown in the **Fig. 3.17**. It is obvious that the higher number of fractures gives larger pseudosteady-state productivity.

However, several cases indicate that productivity of higher number of fractures might be more or less equal or even lower than the productivity of lower number of fractures.

It is also noticeable from that figure, the transient and pseudosteady-state productivity for different number of fractures does not have a stable ratio. For instance, the maximum pseudosteady-state productivity for n_{frac} = 4 is equal to 1.8 with its transient productivity at $t_{DA} = 10^{-6}$ is equal to 9 and the maximum pseudosteady-state productivity for n_{frac} = 2 is equal to 1.2 with its transient productivity at $t_{DA} = 10^{-6}$ is equal to 1.2, thus the ratio of pseudosteady-state productivity to the transient productivity at $t_{DA} = 10^{-6}$ between those two different number of fractures will be 1.5 and 2 respectively.

The transient flow period might be shorter if more fractures are induced to the system, thus the system will be having a lower productivity once the pseudosteady-state flow regime is reached. This fact might be considered in order to choose the appropriate number of induced fractures and well spacing in the manner of field development.

Table 3.3 shows the configurations of the fracture and the productivity for this case. The results show that the productivity of non-fully penetrating fracture might be larger than the fully penetrating ones. This is explained by the fact that width is used to reduce the choke effect and reduced vertical penetration allows to create more width from a given amount of proppant.

Table 3.3 Fracture dimensions and productivity for $k_x = k_y = k_z$

n_{frac}	x_f (ft)	w (ft)	h_f (ft)	N_{prop}	J_D	$J_{D\,total}$	n_{frac}	x_f (ft)	w (ft)	h_f (ft)	N_{prop}	J_D	$J_{D\,total}$
1	660	0.066	100	1	0.502	0.502	4	660	0.016	50	1	0.201	0.804
1	622.3	0.070	100	1	0.543	0.543	4	544.5	0.020	50	1	0.255	1.021
1	641.1	0.070	97	1	0.538	0.538	4	602.3	0.020	45.2	1	0.251	1.003
1	660	0.070	94.2	1	0.536	0.536	4	660	0.020	41.3	1	0.230	0.922
1	544.5	0.080	100	1	0.580	0.580	4	363	0.030	50	1	0.327	1.307
1	602.3	0.080	90.4	1	0.572	0.572	4	511.5	0.030	35.5	1	0.316	1.263
1	660	0.080	82.6	1	0.561	0.561	4	660	0.030	27.5	1	0.271	1.085
1	484	0.090	100	1	0.606	0.606	4	272.3	0.040	50	1	0.368	1.471
1	572	0.090	84.6	1	0.599	0.599	4	466.1	0.040	29.2	1	0.359	1.437
1	660	0.090	73.4	1	0.580	0.580	4	660	0.040	20.6	1	0.304	1.216
1	435.6	0.100	100	1	0.622	0.622	4	217.8	0.050	50	1	0.387	1.546
1	547.8	0.100	79.6	1	0.621	0.621	4	438.9	0.050	24.8	1	0.390	1.559
1	660	0.100	66	1	0.595	0.595	4	660	0.050	16.5	1	0.326	1.303
2	660	0.034	100	1	0.356	0.711	4	181.5	0.060	50	1	0.393	1.573
2	544.5	0.040	100	1	0.423	0.845	4	420.8	0.060	21.6	1	0.411	1.643
2	602.3	0.040	90.4	1	0.414	0.828	4	660	0.060	13.8	1	0.340	1.360
2	660	0.040	82.6	1	0.383	0.767	4	155.6	0.070	50	1	0.393	1.571
2	435.6	0.050	100	1	0.478	0.956	4	407.8	0.070	19.1	1	0.426	1.706
2	547.8	0.050	79.6	1	0.466	0.932	4	660	0.070	11.8	1	0.347	1.389
2	660	0.050	66	1	0.444	0.888	4	136.1	0.080	50	1	0.389	1.555
2	363	0.060	100	1	0.520	1.040	4	398.1	0.080	17.1	1	0.439	1.754
2	511.5	0.060	71	1	0.506	1.012	4	660	0.080	10.3	1	0.353	1.411
2	660	0.060	55	1	0.461	0.923	4	121	0.090	50	1	0.383	1.532
2	311.1	0.070	100	1	0.541	1.083	4	390.5	0.090	15.5	1	0.447	1.790
2	485.6	0.070	64	1	0.537	1.074	4	660	0.090	9.2	1	0.358	1.431
2	660	0.070	47.2	1	0.490	0.980	4	108.9	0.100	50	1	0.377	1.506
2	272.3	0.080	100	1	0.556	1.113	4	384.5	0.100	14.2	1	0.455	1.818
2	466.1	0.080	58.4	1	0.562	1.123	4	660	0.100	8.3	1	0.360	1.441
2	660	0.080	41.2	1	0.504	1.007							
2	242	0.090	100	1	0.559	1.118							
2	451	0.090	53.6	1	0.581	1.162							
2	660	0.090	36.6	1	0.514	1.028							
2	217.8	0.100	100	1	0.556	1.112							
2	438.9	0.100	49.6	1	0.597	1.194							
2	660	0.100	33	1	0.523	1.045							

For the case of non-fully penetrating fracture, the created fracture width which contributes to the overall fracture conductivity might be adequate to provide more production compared to the case of fully penetrating fracture. **Fig. 3.18** below might explains that condition. Detailed results of the productivity of the system with reservoir anisotropy and its comparison with the homogeneous reservoir are shown in **Appendix C.**

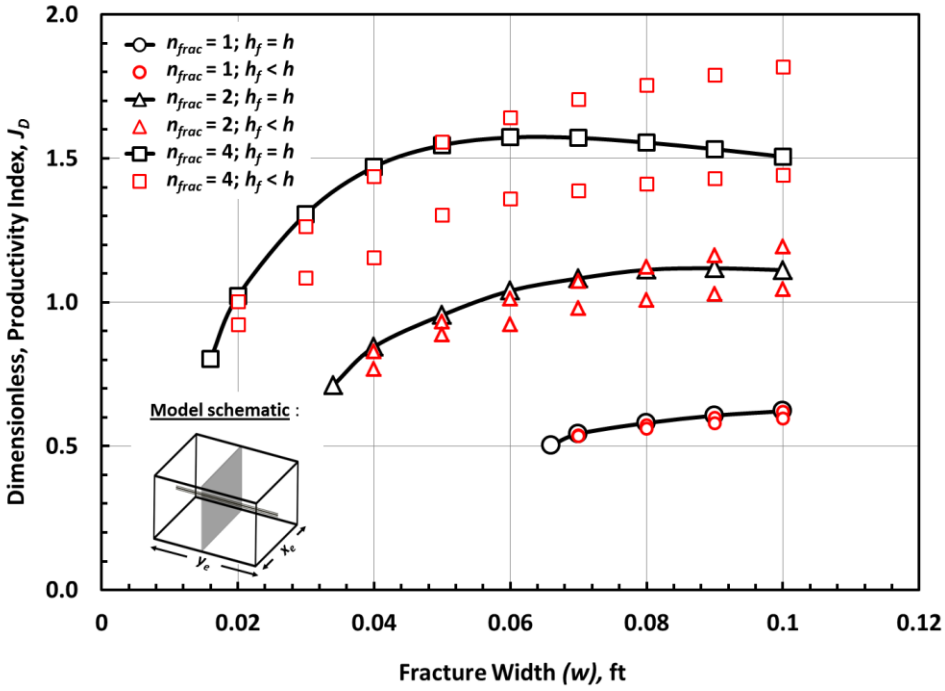

Figure 3.18— Dimensionless productivity index for various n_{frac} as a function of fracture width

Case of $h_f = h$

In this case, the fracture is assumed to be fully penetrating vertically and the vertical permeability is equal to the horizontal permeability. It is obvious that one might always have a gain in productivity by increasing the number of fractures. However at larger number of fractures, n_{frac}, the productivity increase is diminishing. The actual optimum n_{frac} should be determined by net present value optimization..

The maximum productivity is determined for each given proppant number and number of fractures in this section. As like the example case in the previous section, the reservoir volume and dimensions remain the same for various combinations of proppant

number and number of fractures. The total amount of propant will be constant for each given proppant number and being split equally depending on the number of fractures.

Figure 3.19 shows the maximum dimensionless productivity for each given proppant number with number of fractures as a parameter in the system of horizontal well with multiple transverse fractures.

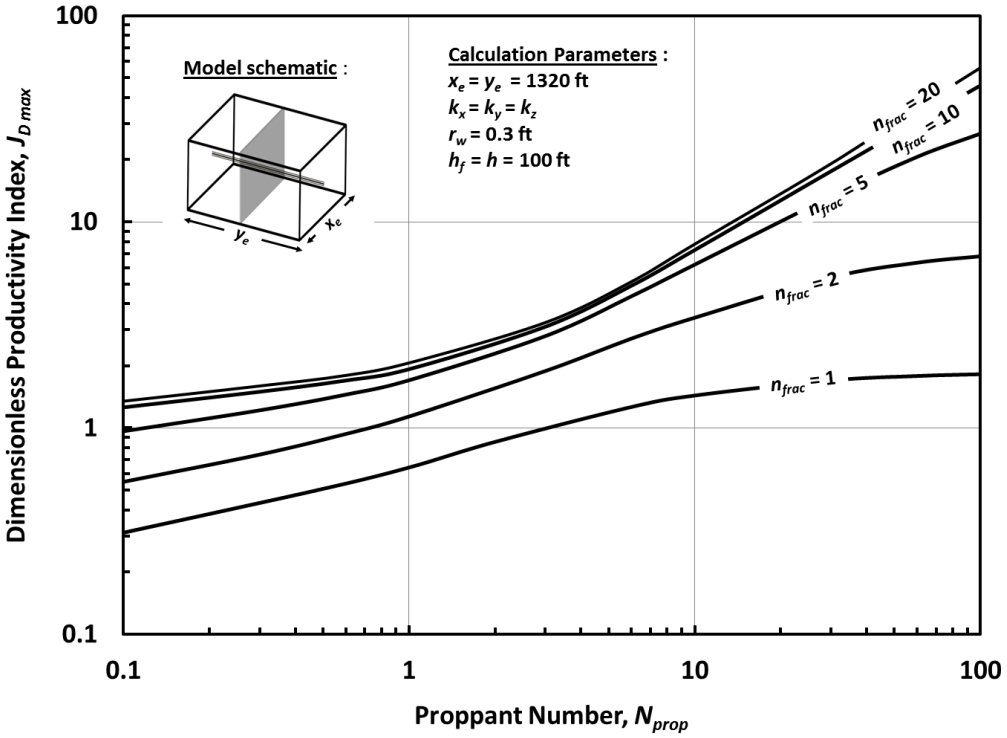

Figure 3.19— Maximum productivity of horizontal well with multiple transverse fractures as a function of N_{prop} with n_{frac} as a parameter

As shown in the figure, the increasing number of productivity increases significantly by inducing fractures in the range of 1 – 5. The increment of productivity gain is smaller for the lower proppant numbers, in other words, increasing the number of fractures and proppant number simultaneously will yield better productivity.

Figure 3.20 shows the maximum productivity as a function of number of fractures with proppant number as a parameter. It shows that the increment of productivity for number of fractures more than 10 is getting smaller for low proppant number.

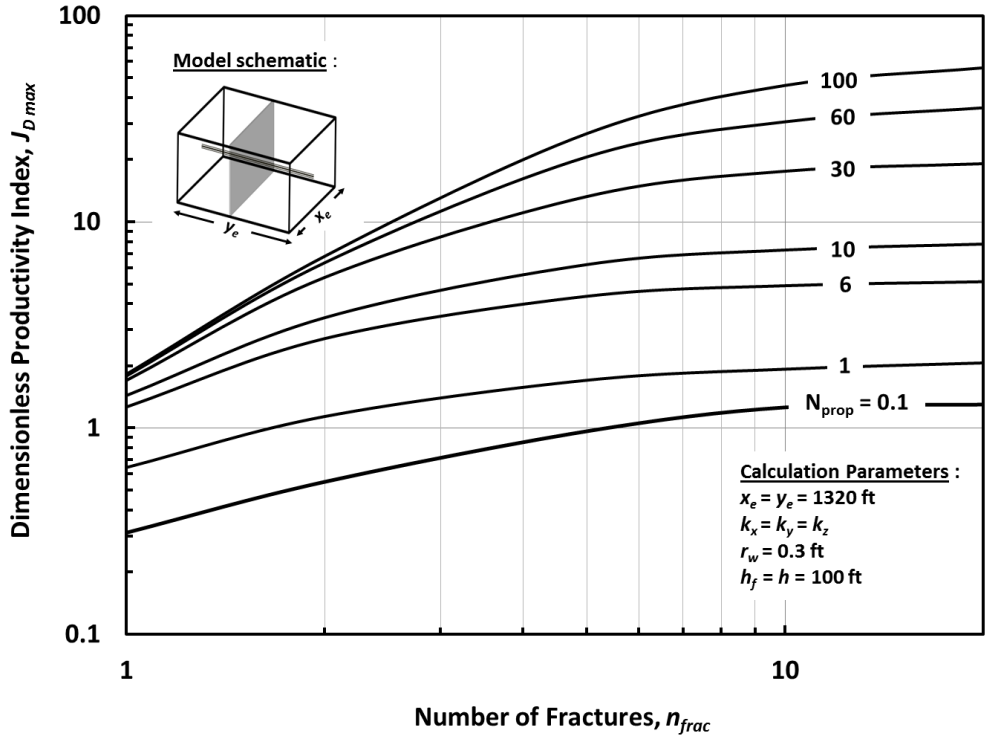

Figure 3.20 — Maximum productivity of horizontal well with multiple transverse fractures as a function of n_{frac} with N_{prop} as a parameter

Daal and Economides (2006) investigated the productivity of hydraulically fractured well in irregular shaped drainage areas. The pseudosteady-state for a vertical well intersected by fully penetrating vertical fracture was calculated by direct boundary method (Romero and Valko, 2003). They found that for the case of proppant numbers

more than 0.1, the optimum dimensionless fracture conductivity for a given proppant number will follow the relation of

$$C_{fD,opt} = \frac{100A_r - C_{fD,0.1}}{100} \times \left(N_p - 0.1\right) + C_{fD,0.1} \quad \text{.....(3.1)}$$

Where $C_{fD,opt}$ is the optimum dimensionless productivity index for each given proppant number; $C_{fD,0.1}$ is the optimum dimensionless fracture conductivity at $N_{prop} = 0.1$ which is given by

$$C_{fD,0.1} = \begin{cases} 1.6 & \text{if } \ 1 \geq \dfrac{1}{A_r} > 0.25 \\ 4.5A_r + 0.25 & \text{if } \ 0.1 \leq \dfrac{1}{A_r} \leq 0.25 \end{cases} \quad \text{.....(3.1)}$$

Figure 3.21 shows the comparison between numerical simulation and the results provided by Daal and Economides for the case of number of fractures equal to 1,2, and 5. It can be concluded from the figure that applying the productivity of hydraulically fractured vertical well into horizontal well case will leads into over-estimation of production.

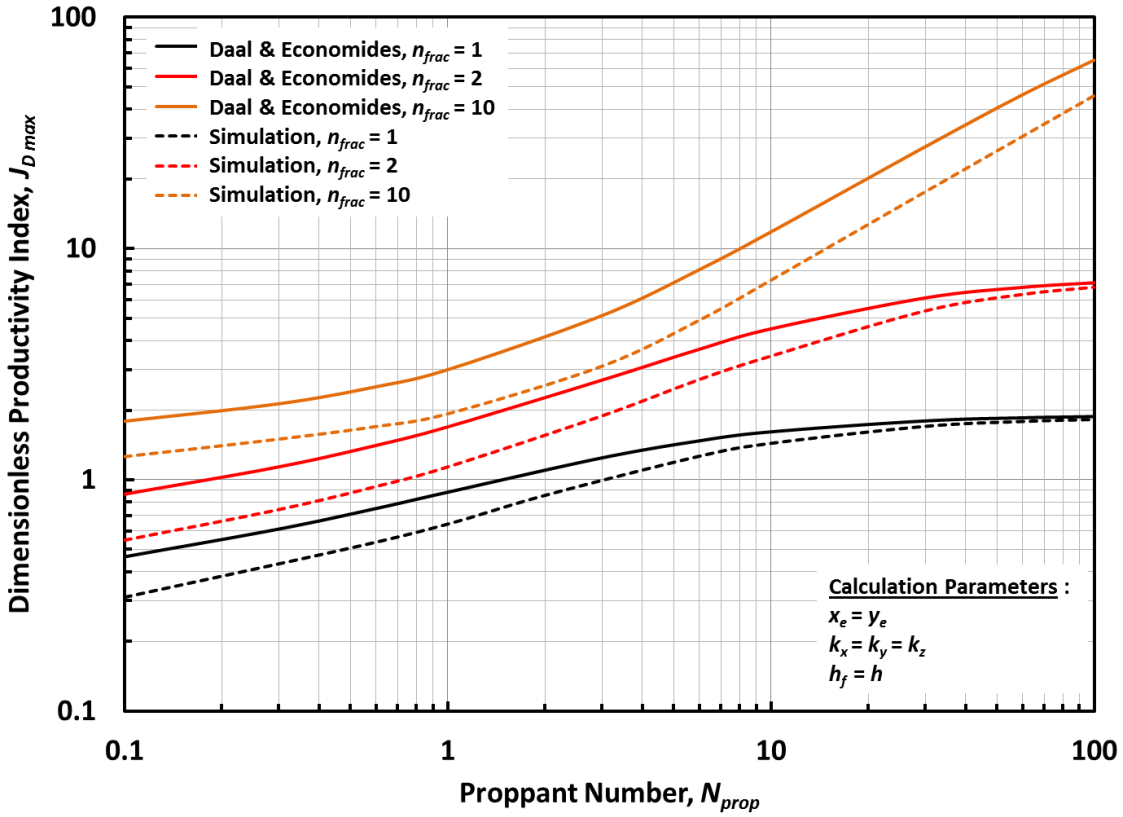

Figure 3.21 — Comparison between numerical simulation and the results provided by Daal and Economides (2006)

3.5 Constant Rate and Constant Pressure Solution

Helmy and Wattenbarger (1998) showed the stabilized dimensionless productivity index does not have the same value for different operating conditions. They found that the productivity for constant pressure is lower than the productivity for constant rate.

The usage of constant rate productivity to predict the performance of a well operated under constant bottomhole pressure will yield over-estimation of the production rate.

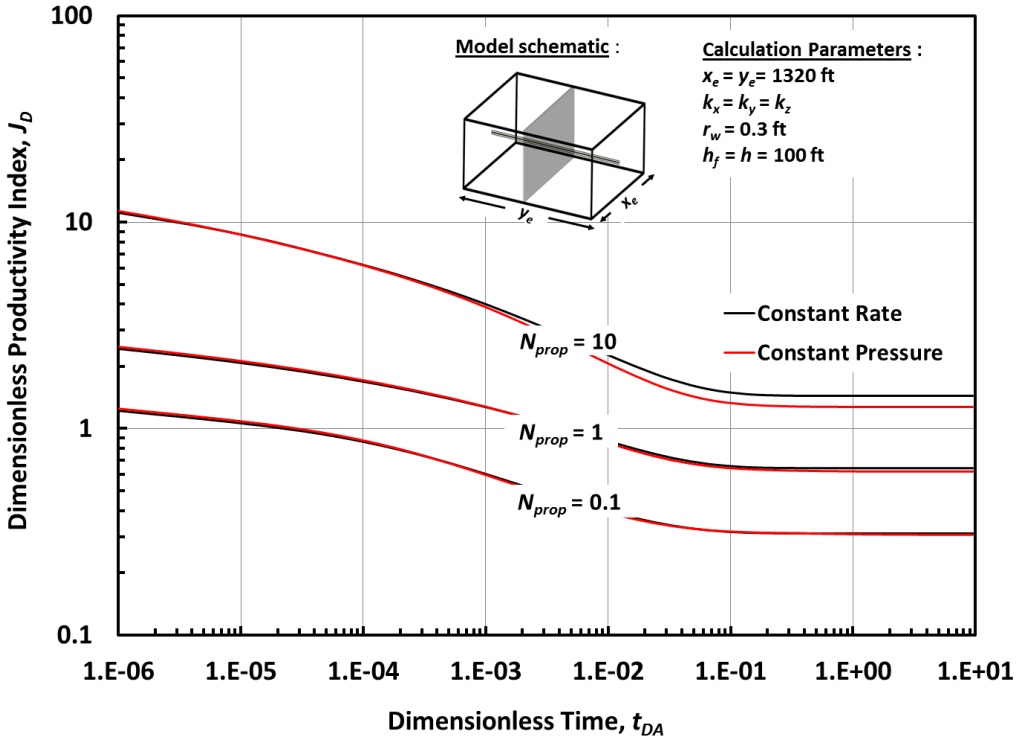

Figure 3.22— Constant rate and constant pressure transient and pseudosteady-state productivity

In this section, the productivity from constant rate and constant pressure solution will be examined as a function of fracture parameters. **Fig. 3.22** shows the transient and pseudosteady-state productivity for a horizontal well with single transverse fracture producing under constant rate and constant pressure operating conditions for N_{prop} equal to 0.1, 1, and 10.

The constant rate productivity is always higher than constant pressure productivity in pseudosteady-state regime and the gap between them is also increasing for higher proppant numbers. Those results are in a good agreement with the statement made by Helmy and Wattenbarger (1998) that the complete linear flow regime will

represents the largest difference between constant rate and constant pressure productivity and it is occurring for high proppant number or high conductivity fracture.

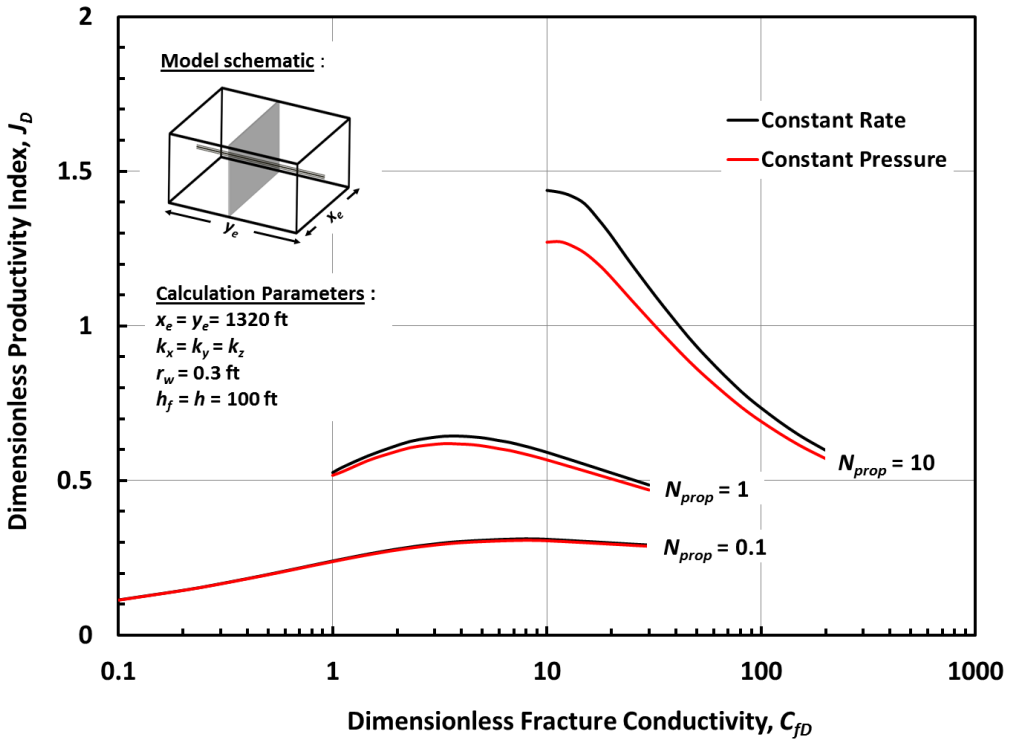

Figure 3.23— Constant rate and constant pressure pseudosteady-state productivity as a function of C_{fD} with N_{prop} as parameter

Figure 3.23 shows the constant rate and constant pressure stabilized productivity as a function of dimensionless fracture conductivity for various proppant numbers. The optimum occurs, however, approximately at the same optimum dimensionless fracture conductivity. The largest difference between those operating conditions occurs at the optimum dimensionless fracture conductivity as well. **Table 3.4** below shows the details of the difference between constant rate and constant pressure productivity for different fracture geometries and proppant numbers.

Table 3.4 - Comparison between constant rate and constant pressure for various fracture dimensions and proppant numbers

n_{frac}	I_x	CfD	Nprop	$J_{D\text{ - Constant Rate}}$	$J_{D\text{ - Constant Pressure}}$	% Diff
1	1.00	0.10	0.1	0.114	0.114	0.53
1	0.71	0.20	0.1	0.145	0.145	0.32
1	0.58	0.30	0.1	0.167	0.166	0.39
1	0.45	0.50	0.1	0.197	0.196	0.53
1	0.35	0.80	0.1	0.226	0.225	0.70
1	0.32	1.00	0.1	0.240	0.238	0.79
1	0.29	1.20	0.1	0.251	0.249	0.87
1	0.27	1.40	0.1	0.260	0.258	0.94
1	0.25	1.60	0.1	0.268	0.265	1.01
1	0.22	2.00	0.1	0.279	0.276	1.11
1	0.19	2.70	0.1	0.292	0.288	1.23
1	0.16	4.00	0.1	0.304	0.299	1.36
1	0.12	7.00	0.1	0.311	0.306	1.47
1	0.10	10.00	0.1	0.310	0.306	1.49
1	0.06	30.00	0.1	0.292	0.288	1.36
1	1.00	1.00	1	0.526	0.517	1.71
1	0.94	1.12	1	0.545	0.531	2.65
1	0.83	1.47	1	0.580	0.565	2.59
1	0.73	1.86	1	0.606	0.588	2.94
1	0.66	2.30	1	0.627	0.606	3.24
1	0.60	2.78	1	0.637	0.615	3.50
1	0.55	3.31	1	0.644	0.620	3.72
1	0.51	3.88	1	0.644	0.618	3.96
1	0.47	4.50	1	0.642	0.616	3.96
1	0.44	5.17	1	0.637	0.611	4.12
1	0.41	6.00	1	0.629	0.603	4.19
1	0.38	7.00	1	0.621	0.595	4.19
1	0.32	10.00	1	0.591	0.567	4.13
1	0.18	30.00	1	0.486	0.470	3.33
1	1.00	10.00	10	1.438	1.271	11.65
1	0.93	11.50	10	1.432	1.272	11.15
1	0.88	13.00	10	1.420	1.247	12.19
1	0.82	15.00	10	1.395	1.236	11.39
1	0.76	17.50	10	1.342	1.197	10.78
1	0.71	20.00	10	1.290	1.156	10.40
1	0.63	25.00	10	1.196	1.081	9.63
1	0.53	35.00	10	1.063	0.971	8.66
1	0.45	50.00	10	0.933	0.862	7.64
1	0.37	75.00	10	0.809	0.756	6.56
1	0.32	100.00	10	0.735	0.691	5.89
1	0.26	150.00	10	0.648	0.615	5.02
1	0.20	250.00	10	0.561	0.538	4.12

CHAPTER IV

FIELD CASE STUDY

4.1 Reservoir and Completion Description

In this section, a case study is performed to see how the numerical solution can be applied to predict the transient and pseudosteady-state productivity index for the field case. Production data in the example case are taken from HPDI database (http://www.hpdi.com/), and the reservoir properties and completion data are taken from published paper (Olsen *et al*., 2009) based on field practice.

'Well A' is located in Williston Basin, North Dakota and has been producing from Bakken Shale formation since 2008 with cumulative oil production nearly 500,000 barrels. This well is selected for the case study because image log shows that the natural fractures in this area will not play an important role to the production due to very small fracture aperture. The well was completed by inducing 6 transverse fractures that intersect the horizontal well. About 300,000 lbs of proppant was placed in the formation, microseismic events indicated the fractures fully penetrates along the reservoir length.

Average reservoir pressure data and operating bottomhole flowing pressure are not available in published papers, the best estimation value is then assumed that the bottomhole flowing pressure for 'Well A' is more or less equal to the bottomhole flowing pressure for other wells in the same field. The production history is shown in the **Fig. 4.1**. The input data are summarized in the **Table 4.1** below.

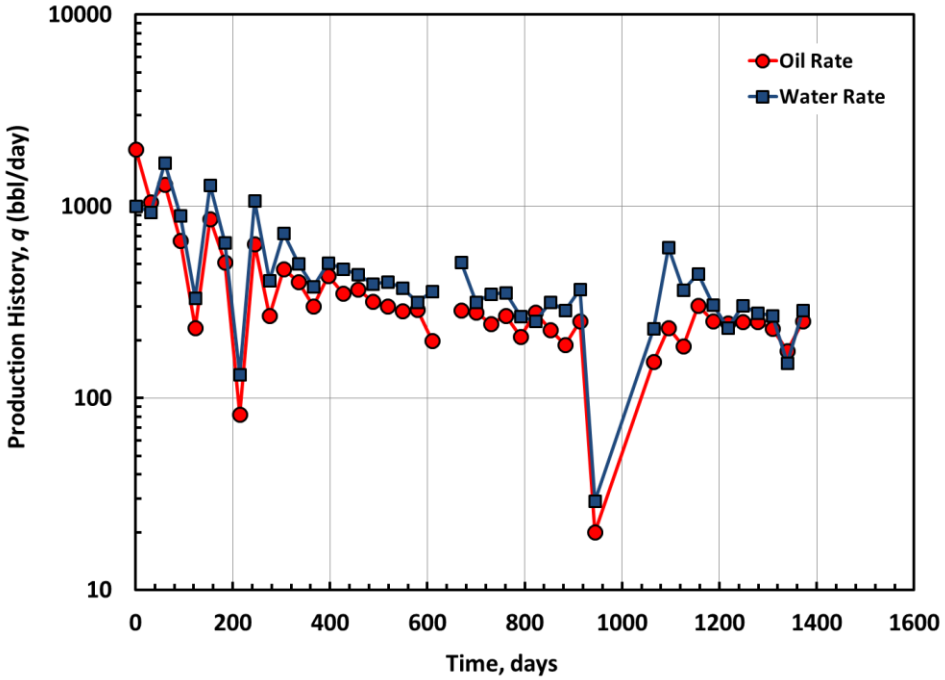

Figure 4.1 — Production history for 'Well A'

Table 4.1 – Reservoir properties and well completion data for 'Well A'

Well Data		
Well Diameter	7	inch
Horizontal Well Length	4,500	ft
Bottomhole Pressure, p_{wf}	1,450	psi
Reservoir Data		
Rock Type	Shale	
Rock Porosity	8%	
Rock Permeability	0.001-0.01	mD
Reservoir Length, x_e	1,500	ft
Reservoir Width, y_e	4,500	ft
Reservoir Height, h	150	ft
Completion Data		
Injected Proppant	300,000	lbs
Proppant SG	2.65	
Number of Fractures, n_f	6	
Fracture Length, x_f	750	ft
Fracture Height, h_f	150	ft

4.2 Methodology and Result

The well is simulated under constant bottomhole flowing pressure which will give the results as the productivity and production rate. For the sake of simplicity, the well is assumed to produce single phase liquid only.The productivity index in this case will be the total liquid production which consists of oil and water (by assuming gas production is the associated gas) divided by the pressure drop as shown in Eq. 4.1 below.

$$J = \frac{q_0 + q_w}{p_{ave} - p_{wf}} \quad \text{.....(4.1)}$$

The simulated productivity index and dimensionless productivity index as a function of time and dimensionless time based on drainage area and productivity index in the dimensionless variable are shown in the **Fig. 4.2.**

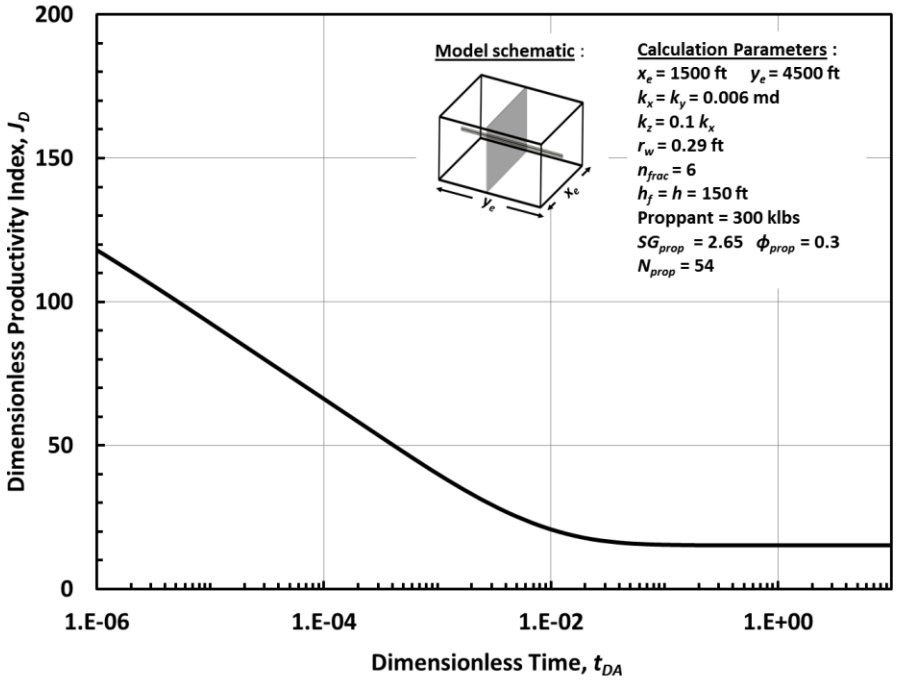

Figure 4.2 — Transient and pseudosteady-state productivity for 'Well A' case

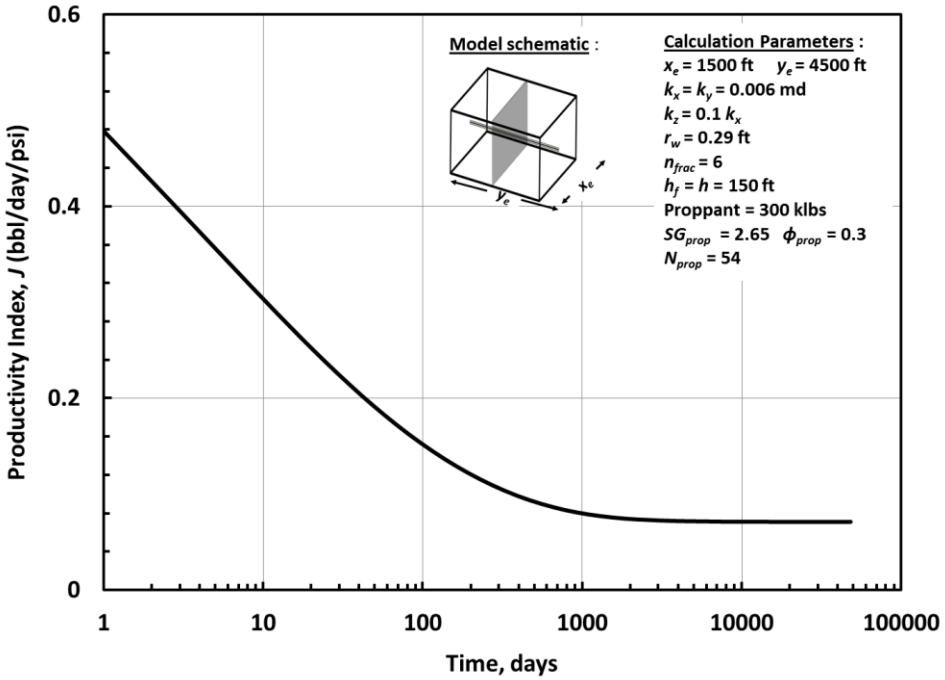

Figure 4.2 — Continued

It can be seen from the figures that the productivity of 'Well A' is starting to stabilize after producing more than 2000 days. The current producing time is nearly 1500 days, thus it can be concluded that 'Well A' is still producing under the transient regime. The usage of pseudosteady-state productivity to predict the performance of this well might leads into under-estimate production rate.

The proppant properties were not clearly described in the reference, then we assume that the proppant permeability, k_f, is within the range of 30000–50000 md; and the proppant pack porosity, ϕ_f, is 30%. The total effective compressibility is equal to 1.18×10^{-5} 1/psi and it is assumed to be constant during depletion. We assumed that average viscosity is equal to 0.48 cp and vertical – horizontal permeability contrast is equal to 0.1.

The reservoir and fracture permeability are the parameters which were used to produce a good match between historical production data and numerical simulation result. The production rate computed by numerical simulation indicates a good agreement with the production history as shown in **Figs. 4.3** and **4.4** below by assuming the proppant permeability is equal to 30000 md and reservoir permeability is equal to 0.006 md.

We can see the effect of well shut in which was happened from day 900 until day 1100, the liquid production was going up after that period due to pressure build-up. However, the decline trends for both production history and simulation result still in a good agreement after that point.

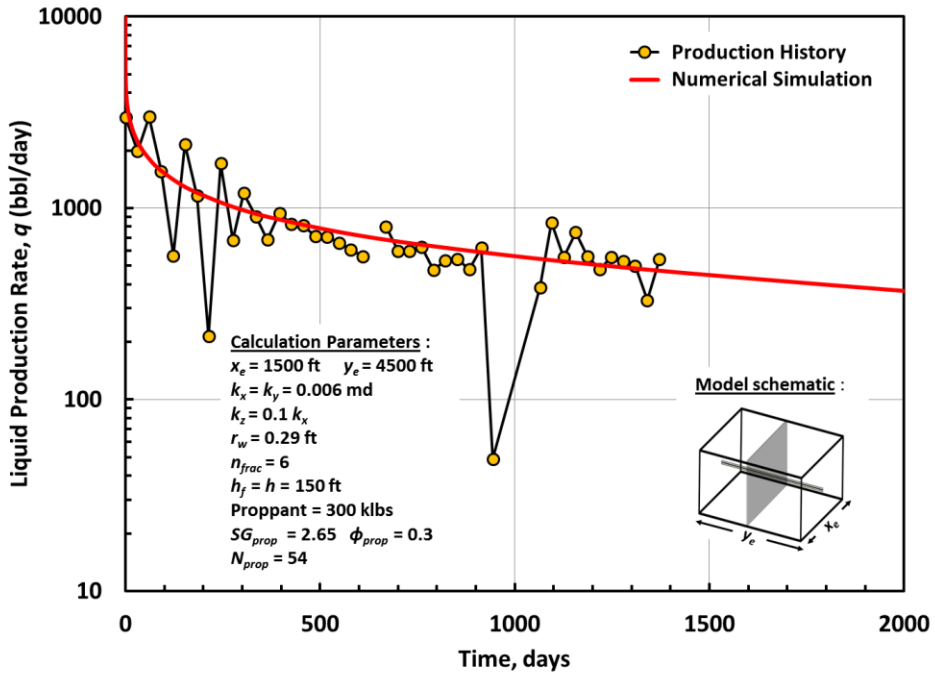

Figure 4.3 — Numerical simulation result and production history in semi-log plot

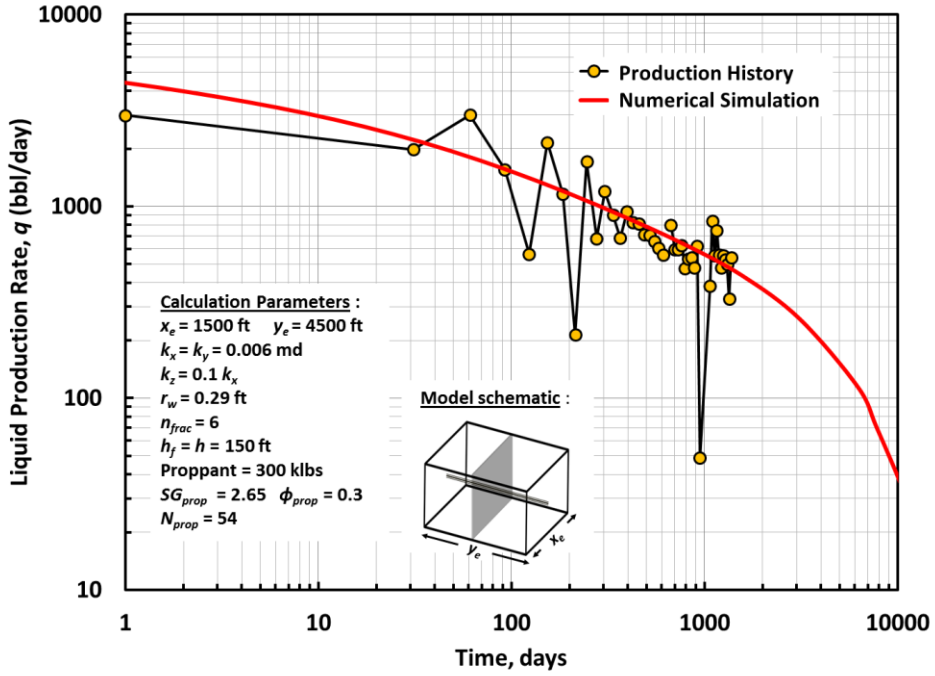

Figure 4.4 — Numerical simulation result and production history in log-log plot

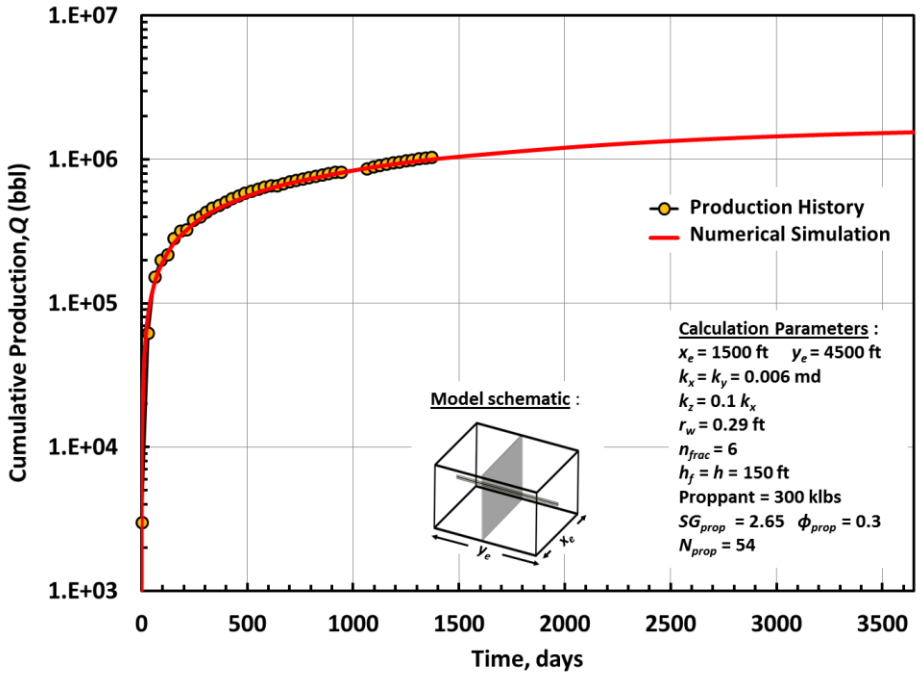

Figure 4.5 — 10-years cumulative liquid production forecasting

Figure 4.5 above shows the qumulative liquid production matching and forecasting for 10 years. The forecasted 10-years cumulative liquid production is around 1.6 MMbbl, note that the liquid consists of oil and water and the water rate will be increasing during production time.

There is possibility that the fractures that have been induced in this reservoir do not meet the optimum design, thus the sensitivity analysis will be performed in order to analyze the better fracture design for this well. First of all, we assume the amount of proppant remains the same (N_{prop} = 54). The first case is to analyze whether the fracture dimensions (length and width termed by I_x and C_{fD}) already close to the optimum design which yield maximum productivity. The number of fractures for this case will remain the same (n_{frac} = 6), and hopefully we would see the optimum fracture dimensions by varying lateral fracture penetration and fracture width.

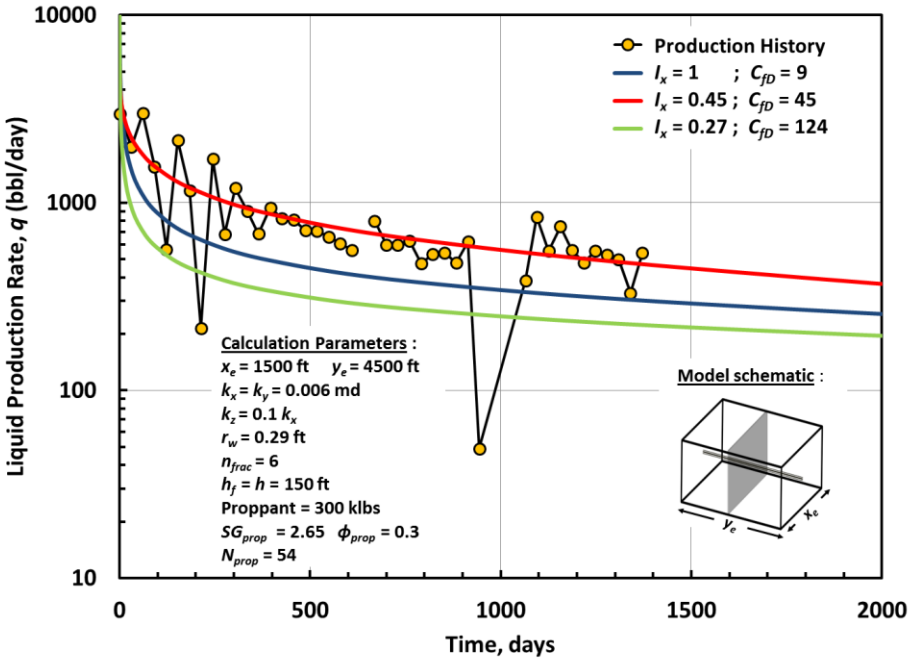

Figure 4.6 — Production rate for various fracture dimensions, n_{frac} = 6

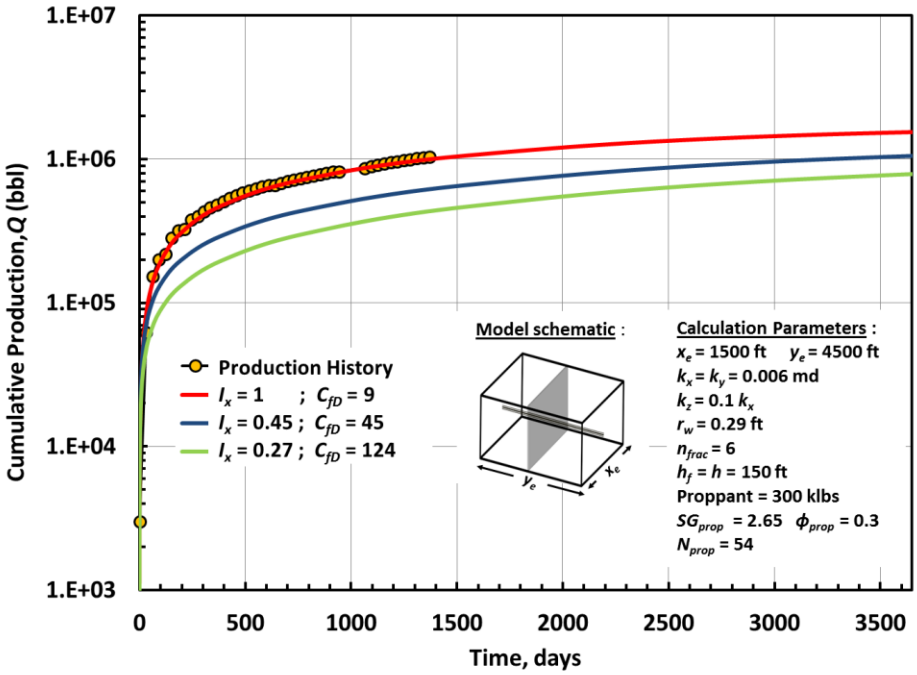

Figure 4.7 — 10-years cumulative liquid production forecasting, various fracture dimensions, n_{frac} = 6

From the **Figs. 4.6** and **4.7**, we can see that the current fracture dimension provides the best productivity. The cumulative liquid production after 10 years will be decreasing as we reduce the lateral fracture penetration or increase the fracture width.

The second case is to analyze the production gain by increasing the number of fractures. As mentioned before, the proppant number and will remains the same, and the transverse fractures in this case will be assumed fully penetrating laterally. The next figures will show the improvement in productivity as number of fractures increases. It can be seen from **Fig. 4.8** below that for larger number of fractures, the production rate declines faster than the case of smaller number of fractures at late production time.

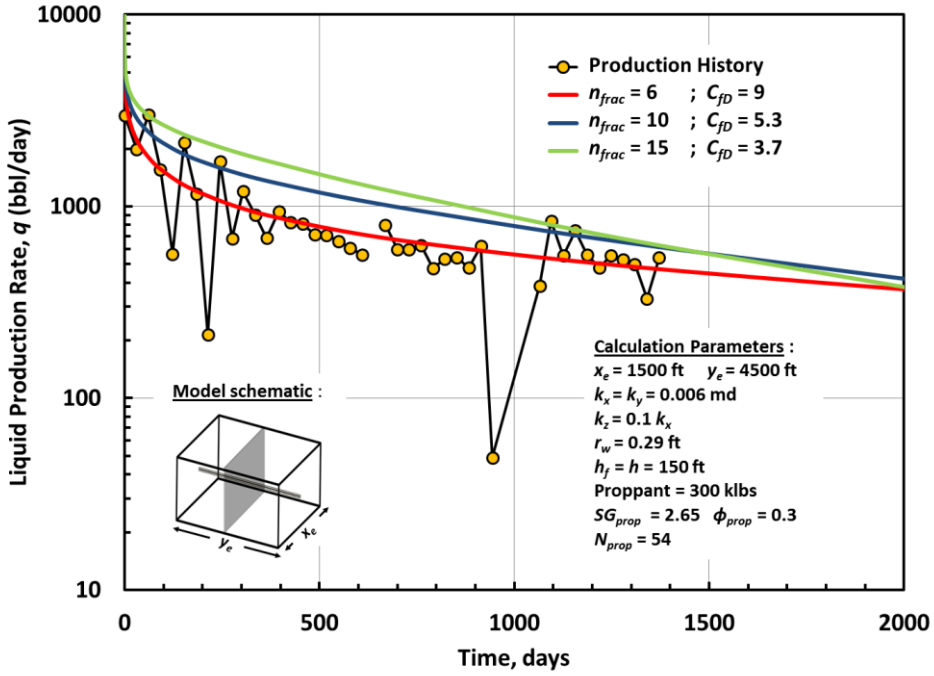

Figure 4.8 — Production rate for various number of fractures, I_x = 1

The figure also shows the productivity increases significantly by increasing number of fractures especially during the early production time. This result proves that depletion will be occurred rapidly by inducing more fractures.

As mentioned before in the previous chapter, inducing more fractures in the reservoir will increase the productivity of the horizontal well. The 10-years cumulative production can be used as a parameter to decide the appropriate number of fractures for a particular well-reservoir system. It is clearly seen on **Fig. 4.9** that increasing the number of fractures provides more cumulative recovery (faster recovery) during early production time. However the difference of 10-years cumulative production for number of fractures equal to 10 and 15 is not significant.

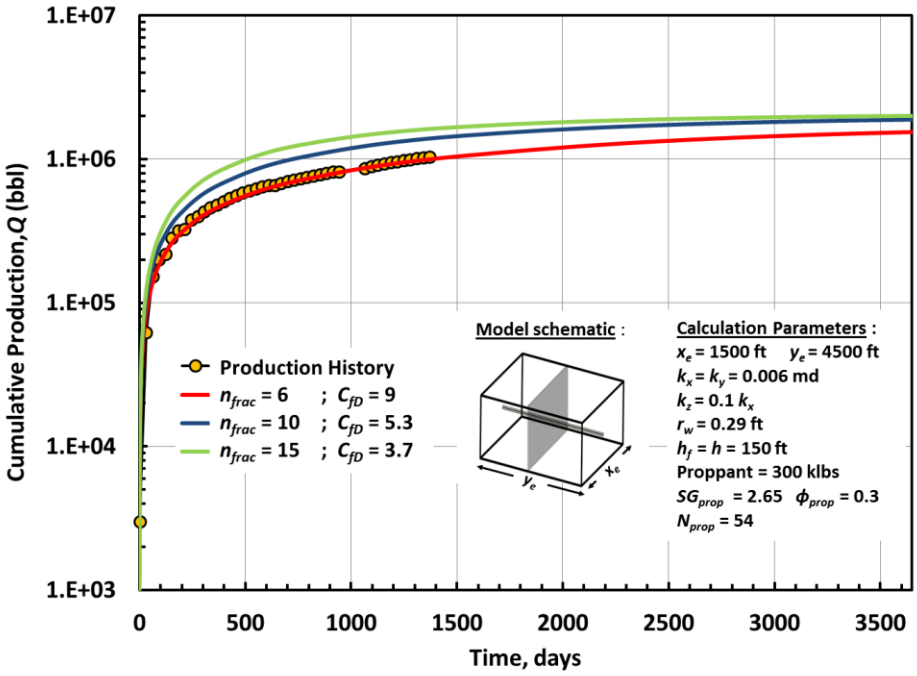

Figure 4.9 — 10-years cumulative liquid production forecasting, various number of fractures, I_x = 1

CHAPTER V

SUMMARY AND RECOMMENDATIONS

5.1 Summary

Numerical simulation model has been applied to predict the transient and pseudosteady-state productivity for various reservoir, wellbore, and fracture geometries including the model of horizontal well with multiple transverse fractures in rectangular drainage area. The pressure and productivity behavior calculated by this method are validated with various existing solutions.

Numerical experimentation reveals that the relation of equivalent wellbore radius in the gridblock, $x_0 = 0.4\ r_w$, provides the best result of shape factors with this numerical simulator if logarithmic increasing gridblock size ("logarithmic mesh") is used.

The results provide a more accurate characterization of the choking effect at the intersection between wellbore and transverse fractures. However, the productivity penalty due to choke skin might be reduced by improvement in proppant number (increasing volume or quality of the proppant).

The productivity of the well producing under constant bottomhole flowing pressure is smaller than in the case of constant rate. Hence applying the productivity of constant rate solution to the constant pressure case will yields into over-estimation of production. However, the optimum stabilized productivity of fractured well for both operating conditions occur approximately at the same dimensionless fracture conductivity and the largest difference is discovered at the optimum point.

The developed simulator was shown to be a powerful tool to predict the transient and pseudosteady-state productivity for such a complex well-fracture system in an actual field case. Further calculation revealed the possibility to improve the completion design by increasing the number of fractures while keeping the proppant amount unchanged.

5.2 Recommendations

The results show that performance of horizontal well intersected by multiple transverse fractures could be improved by increasing the number of fractures. However, the optimization of net present value will provide the actual optimum number of fractures. It can be concluded from the field case example that increasing number of fractures will expedite the production during early time.

The numerical simulator was developed in a way to increase the reusability and the easiness of expansion. Thus, the single phase numerical simulator can be easily modified into multiphase simulator by implementing the concepts of capillary pressure and relative permeability. Such an extension will provide an efficient tool for completion optimization in case where multiphase flow effects are significant.

REFERENCES

Al-Kobaisi, M., Ozkan, E., and Kazemi, H. 2006. A Hybrid Numerical/Analytical Model of a Finite-Conductivity Vertical Fracture Intercepted by a Horizontal Well. *SPE Reservoir Evaluation & Engineering* **9** (4): 345-355. doi: 10.2118/92040-pa

Chen, C.-C. and Raghavan, R. 1997. A Multiply-Fractured Horizontal Well in a Rectangular Drainage Region. *SPE Journal* **2** (4): 455-465. doi: 10.2118/37072-pa

Daal, J.A. and Economides, M.J. 2006. Optimization of Hydraulically Fractured Wells in Irregularly Shaped Drainage Areas. Paper SPE-98047-MS presented at the International Symposium and Exhibition on Formation Damage Control, Lafayette, Louisiana, 15-17 February. doi: 10.2118/98047-ms

Dietz, D.N. 1965. Determination of Average Reservoir Pressure from Build-up Surveys. *Journal of Petroleum Technology* **17** (8): 955-959. doi: 10.2118/1156-pa

Durlofsky, L.J. 1991. Numerical Calculation of Equivalent Grid Block Permeability Tensors for Heterogeneous Porous Media. *Water Resour. Res.* **27** (5): 699-708. doi: 10.1029/91WR00107

Economides, M.J., Oligney, R.E., and Valkó, P.P.: *Unified Fracture Design*, Orsa Press, Alvin, Texas (2002).

Gringarten, A.C., Henry J. Ramey, J., and Raghavan, R. 1974. Unsteady-State Pressure Distributions Created by a Well with a Single Infinite-Conductivity Vertical Fracture. *SPE Journal* **14** (4): 347-360. doi: 10.2118/4051-pa

Helmy, M.W. and Wattenbarger, R.A. 1998. New Shape Factors for Wells Produced at Constant Pressure. Paper SPE-39970-MS presented at the SPE Gas Technology Symposium, Calgary, Alberta, Canada, 15-18 March. doi: 10.2118/39970-ms

Meyer, B.R., Bazan, L.W., Jacot, R.H., Lattibeaudiere, M.G. 2010. Optimization of Multiple Transverse Hydraulic Fractures in Horizontal Wellbores. Paper SPE-131732-MS presented at the SPE Unconventional Gas Conference, Pittsburgh, Pennsylvania, 23-25 February. doi: 10.2118/131732-ms

Moridis, G.J. 2011. "PETE 640 Class Notes," Petroleum Engineering Department, Texas A&M University, Texas.

Mukherjee, H. and Economides, M.J. 1991. A Parametric Comparison of Horizontal and Vertical Well Performance. *SPE Formation Evaluation* **6** (2): 209-216. doi: 10.2118/18303-pa

Olsen, T.N., Gomez, E., McCrady, D.D., Forrest, G., Perrakis, A., et al. 2009. Stimulation Results and Completion Implications from the Consortium Multi-Well Project in the North Dakota Bakken Shale. Paper SPE-124686-MS presented at the SPE Annual Technical Conference and Exhibition, New Orleans, Louisiana, 4-7 October. doi: 10.2118/124686-ms

Ozkan, E. and Raghavan, R. 1991. New Solutions for Well-Test-Analysis Problems: Part 1 - Analytical Considerations (Includes Associated Papers 28666 and 29213). *SPE Formation Evaluation* **6** (3): 359-368. doi: 10.2118/18615-pa

Peaceman, D.W., Interpretation of Well-Block Pressures in Numerical Reservoir Simulation (Includes Associated Paper 6988). *SPE Journal* **18** (3): 183-194. doi: 10.2118/6893-pa

Pruess, K. 1991. TOUGH2: A general numerical simulator for multiphase fluid and heat flow. Lawrence Berkeley Laboratory Report LBL-29400, Berkeley, California.

Raghavan, R.: Well Test Analysis, Prentice Hall, Englewood Cliffs, New Jersey, 1993.

Romero, D.J., Valko, P.P., and Economides, M.J. 2002. The Optimization of the Productivity Index and the Fracture Geometry of a Stimulated Well with Fracture Face and Choke Skins. Paper SPE-73758-MS presented at the International Symposium and Exhibition on Formation Damage Control, Lafayette, Louisiana, 20-21 February. doi: 10.2118/73758-ms

Sabaev, V.V., Wolcott, D.S., Mach, J.M., Antipina D.V., Haidar, A.M. et al. 2006. Vertically Fractured Well Performance in Rectangular Drainage Area. Paper SPE-101048-MS presented at the SPE Russian Oil and Gas Technical Conference and Exhibition, Moscow, Russia, 3-6 October. doi: 10.2118/101048-ms

Valko, P.P. and Amini, S. 2007. The Method of Distributed Volumetric Sources for Calculating the Transient and Pseudosteady-State Productivity of Complex Well-Fracture Configurations. Paper SPE-106279-MS presented at the SPE Hydraulic Fracturing Technology Conference, College Station, Texas, 29-31 January. doi: 10.2118/106279-ms

APPENDIX A

DEVELOPMENT OF NUMERICAL SIMULATION MODEL

Reservoir simulation code is developed and modified specifically for this work purposes from TOUGH family of simulation tools for flow and transport processes in porous media (Pruess, 1991) which is originally developed by researchers in Earth Sciences division of Lawrence Berkeley National Laboratory and written in FORTRAN 95. The TOUGH simulator was developed with Object-Oriented Programming (OOP) technique to increase the reusability and maintainability of the source code and also the easiness of expansion.

Mass balance for single phase and single component fluid in every subdomain is subdivided by the integral of finite difference (Pruess *et al*., 1999).

$$\frac{d}{dt}\int_{V_n} M\, dV = \int_{\Gamma_n} F \cdot n\, d\tilde{A} + \int_{V_n} q\, dV \quad \text{..... (A.1)}$$

Where,

M = mass accumulation term, kg/m^3

V = volume, L^3

V_n = volume of subdomain n, L^3

A = surface area, L^2

Γ_n = surface area of subdomain n, L^2

F = Darcy flux vector, $kg\ m^{-2}s^{-1}$

n = inward unit normal vector

q = source or sink term, $kg\ m^{-3}s^{-1}$

t = time, T

The mass accumulation terms, M, is expressed as

$$M = \phi \rho \quad \text{(A.2)}$$

Where,

ϕ = porosity

ρ = fluid density, kg/m^3

Assuming Darcy's flow, the mass flux for single phase and single component fluid is expressed as

$$F = -k \frac{\rho}{\mu} \left(\nabla P - \rho g \right) \quad \text{(A.3)}$$

Where,

k = permeability, m^2

μ = fluid viscosity, $Pa\ s$

P = pressure, Pa

g = gravitational acceleration, $m\ s^{-2}$

Equation A.1 is also discretized in space, introducing the appropriate volume averages,

$$\int_{V_n} M \, dV = V_n \, M_n \quad \text{(A.4)}$$

where M_n is the average value of M_n over V_n. The flux term in the right hand side of Eq. A.1 is approximated as discrete sum of average flux on the surface segments A_{nm},

$$\int_{\Gamma_n} F \cdot n \, d\Gamma = \sum_m A_{nm} F_{nm} \quad \text{(A.5)}$$

Assuming Darcy's flow, the discretized flux is expressed in terms of averages of parameters for elements *n* and *m*,

$$F_{nm} = -k_{nm}\left\lfloor \frac{\rho}{\mu} \right\rfloor_{nm}\left(\frac{P_n - P_m}{D_{nm}} - \rho_{nm}\, g_{nm} \right) \quad \text{(A.6)}$$

The subscript *nm* is expressing a suitable averaging at the interface between subdomains *n* and *m* which in this study will be the harmonic averaging. D_{nm} represents the distance between nodal points in subdomain *n* and *m*.

Substituting Eq. A.6 into Eq. A.1 gives

$$\frac{dM_n}{dt} = \frac{1}{V_n}\sum_m A_{nm}F_{nm} + q_n \quad \text{(A.7)}$$

The flux and source or sink terms on the right hand side of **Eq. A.7** are evaluated at the new time level, $t^{k+1} = t^k + \Delta t$, so the fluxes are expressed in terms of the unknown parameters at time t^{k+1}, this treatment is known as *fully implicit*.

The time discretization yields into the set of non-linear equation as follow

$$R_n^{k+1} = M_n^{k+1} - M_n^{k} - \frac{\Delta t}{V_n}\left(\sum_m A_{nm}F_{nm}^{k+1} + V_n q_n^{k+1} \right) = 0 \quad \text{(A.8)}$$

where R_n^{k+1} represents the residuals. Each subdomain has one equation for single phase and single component fluid, and isothermal condition as being assumed in this study, thus there will be *N* equation to solve for *N* grid blocks. The **Eq. A.8** is solved by Newton Raphson iteration.

APPENDIX B

RESULTS OF CALCULATION FOR DIMENSIONLESS PRODUCTIVITY INDEX FOR VARIOUS N_{prop}, n_{frac} = 1

Table B.1 Productivity for various fracture geometry and proppant number

N_{prop}	I_x	C_{fD}	J_D	N_{prop}	I_x	C_{fD}	J_D
0.05	1.000	0.05	0.070	0.5	1.000	0.5	0.341
0.05	0.707	0.1	0.089	0.5	0.707	1.0	0.419
0.05	0.316	0.5	0.155	0.5	0.598	1.4	0.453
0.05	0.224	1	0.190	0.5	0.559	1.6	0.465
0.05	0.158	2	0.223	0.5	0.500	2	0.482
0.05	0.129	3	0.239	0.5	0.408	3	0.502
0.05	0.112	4	0.248	0.5	0.354	4	0.507
0.05	0.091	6	0.256	0.5	0.302	5.5	0.505
0.05	0.079	8	0.260	0.5	0.267	7	0.498
0.05	0.071	10	0.261	0.5	0.250	8	0.492
0.05	0.060	14	0.261	0.5	0.224	10	0.482
0.05	0.050	20	0.259	0.5	0.158	20	0.440
0.05	0.035	40	0.251	0.5	0.112	40	0.397
0.05	0.022	100	0.235	0.5	0.071	100	0.345
0.05	0.011	400	0.207	0.5	0.035	400	0.285
0.05	0.007	1000	0.193	0.5	0.022	1000	0.257
0.1	1.000	0.1	0.114	1	1.000	1	0.526
0.1	0.447	0.5	0.197	1	0.825	1.5	0.580
0.1	0.354	0.8	0.226	1	0.733	1.9	0.606
0.1	0.316	1.0	0.240	1	0.660	2.3	0.627
0.1	0.267	1.4	0.260	1	0.600	2.8	0.637
0.1	0.250	1.6	0.268	1	0.550	3.3	0.644
0.1	0.236	1.8	0.274	1	0.508	3.9	0.644
0.1	0.224	2.0	0.279	1	0.471	4.5	0.642
0.1	0.192	3	0.292	1	0.440	5.2	0.637
0.1	0.158	4	0.304	1	0.408	6	0.629
0.1	0.120	7	0.311	1	0.378	7	0.621
0.1	0.100	10	0.310	1	0.316	10	0.591
0.1	0.058	30	0.292	1	0.183	30	0.486
0.1	0.032	100	0.261	1	0.100	100	0.390
0.1	0.016	400	0.227	1	0.050	400	0.315
0.1	0.010	1000	0.204	1	0.032	1000	0.280

Table B.1 Continued

N_{prop}	I_x	C_{fD}	J_D	N_{prop}	I_x	C_{fD}	J_D
2	1.000	2	0.784	10	1.000	6.0	1.265
2	0.933	2.3	0.809	10	0.933	6.9	1.263
2	0.877	2.6	0.827	10	0.877	7.8	1.255
2	0.816	3.0	0.843	10	0.816	9.0	1.243
2	0.756	3.5	0.854	10	0.756	10.5	1.220
2	0.707	4	0.857	10	0.707	12	1.186
2	0.632	5	0.851	10	0.632	15	1.118
2	0.535	7	0.826	10	0.535	21	1.013
2	0.447	10	0.779	10	0.447	30.0	0.903
2	0.365	15	0.716	10	0.365	45	0.791
2	0.316	20	0.670	10	0.316	60	0.723
2	0.258	30	0.608	10	0.258	90	0.641
2	0.200	50	0.540	10	0.200	150	0.558
2	0.141	100	0.464	10	0.155	250	0.492
2	0.100	200	0.405	10	0.131	350	0.456
2	0.071	400	0.360	10	0.110	500	0.424
2	0.045	1000	0.315	10	0.077	1000	0.373
6	1.000	6	1.265	30	1.000	30	1.703
6	0.933	6.9	1.263	30	0.933	34.5	1.684
6	0.877	7.8	1.255	30	0.877	39.0	1.650
6	0.816	9.0	1.243	30	0.816	45.0	1.579
6	0.756	10.5	1.220	30	0.756	52.5	1.496
6	0.707	12	1.186	30	0.707	60.0	1.418
6	0.632	15	1.118	30	0.632	75.0	1.288
6	0.535	21	1.013	30	0.535	105.0	1.119
6	0.447	30	0.903	30	0.447	150.0	0.966
6	0.365	45	0.791	30	0.365	225.0	0.827
6	0.316	60	0.723	30	0.316	300	0.747
6	0.258	90	0.641	30	0.258	450	0.655
6	0.200	150	0.558	30	0.200	750	0.565
6	0.155	250	0.492	30	0.173	1000	0.520
6	0.131	350	0.456				
6	0.110	500	0.424				
6	0.077	1000	0.373				

Table B.1 Continued

N_{prop}	I_x	C_{fD}	J_D	N_{prop}	I_x	C_{fD}	J_D
60	1.000	60	1.788	100	1.000	100	1.824
60	0.933	69	1.760	100	0.933	115	1.792
60	0.877	78	1.702	100	0.877	130	1.732
60	0.816	90	1.635	100	0.816	150	1.658
60	0.756	105	1.541	100	0.756	175	1.559
60	0.707	120	1.455	100	0.707	200	1.470
60	0.632	150	1.314	100	0.632	250	1.325
60	0.535	210	1.134	100	0.535	350	1.140
60	0.447	300	0.975	100	0.447	500	0.979
60	0.365	450	0.832	100	0.365	750	0.834
60	0.316	600	0.751	100	0.316	1000	0.752
60	0.258	900	0.657				
60	0.245	1000	0.640				

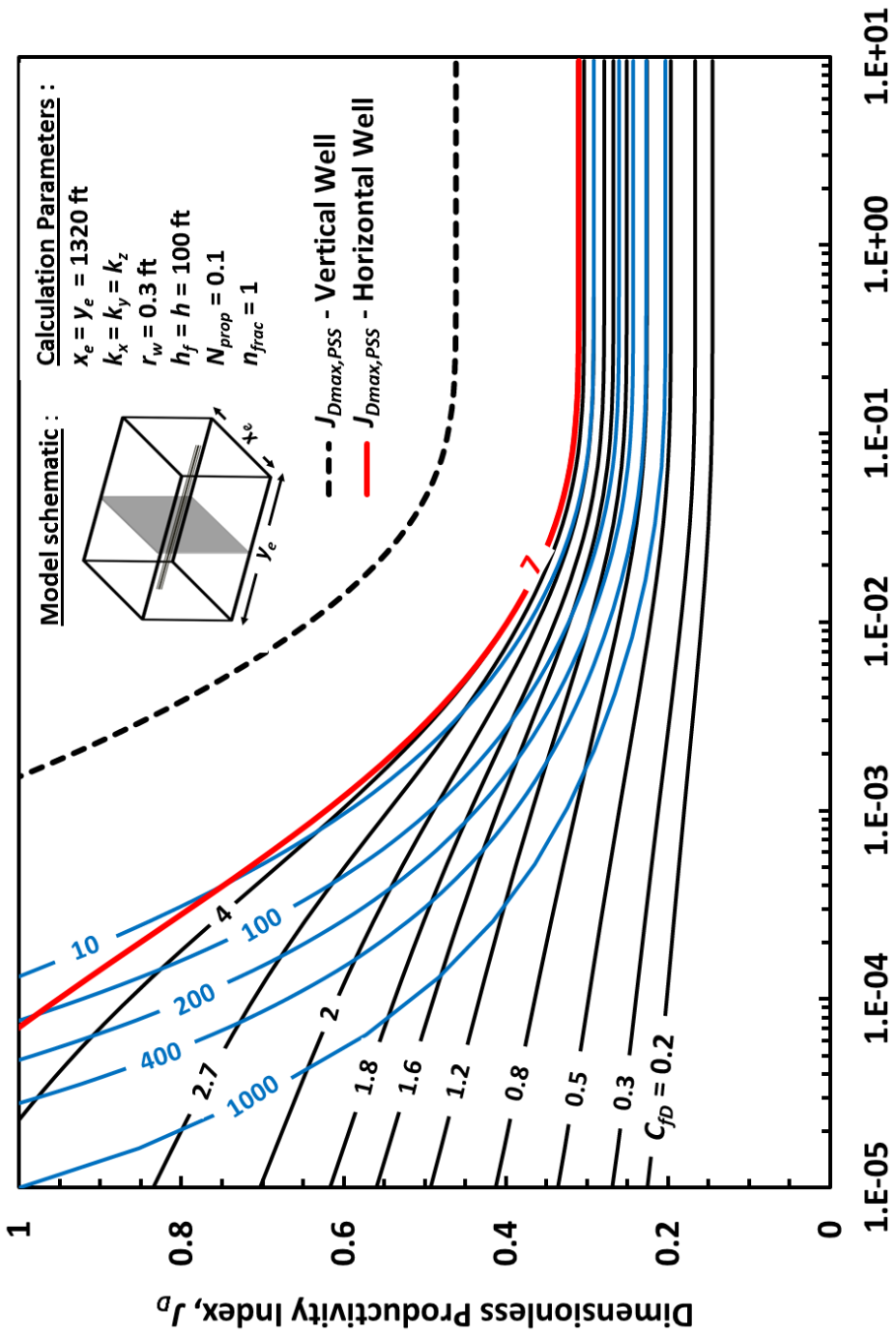

Figure B.1 — Transient and Pseudosteady-state productivity of horizontal well with transverse fracture, N_{prop} = 0.1

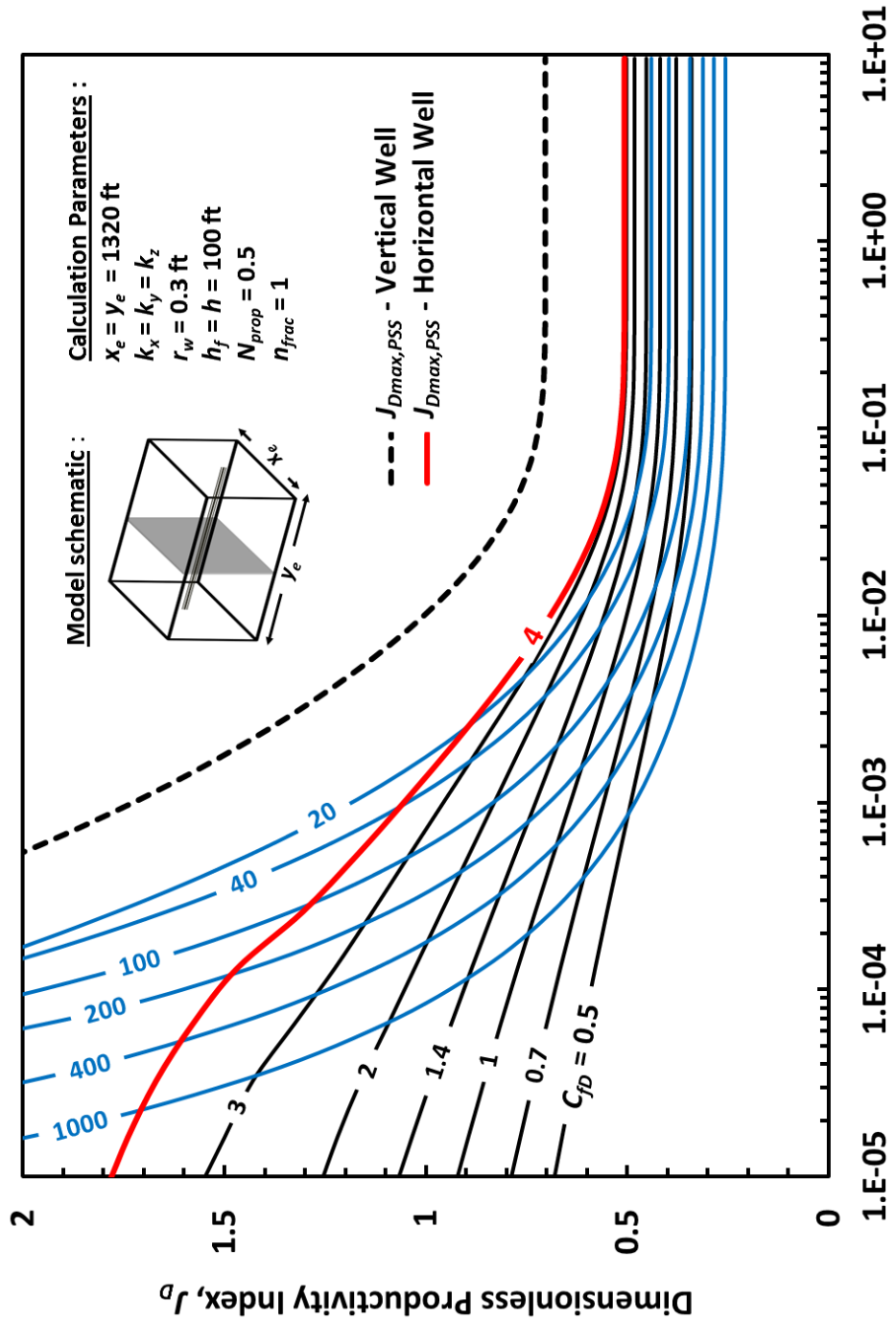

Figure B.2 — Transient and Pseudosteady-state productivity of horizontal well with transverse fracture, N_{prop} = 0.5

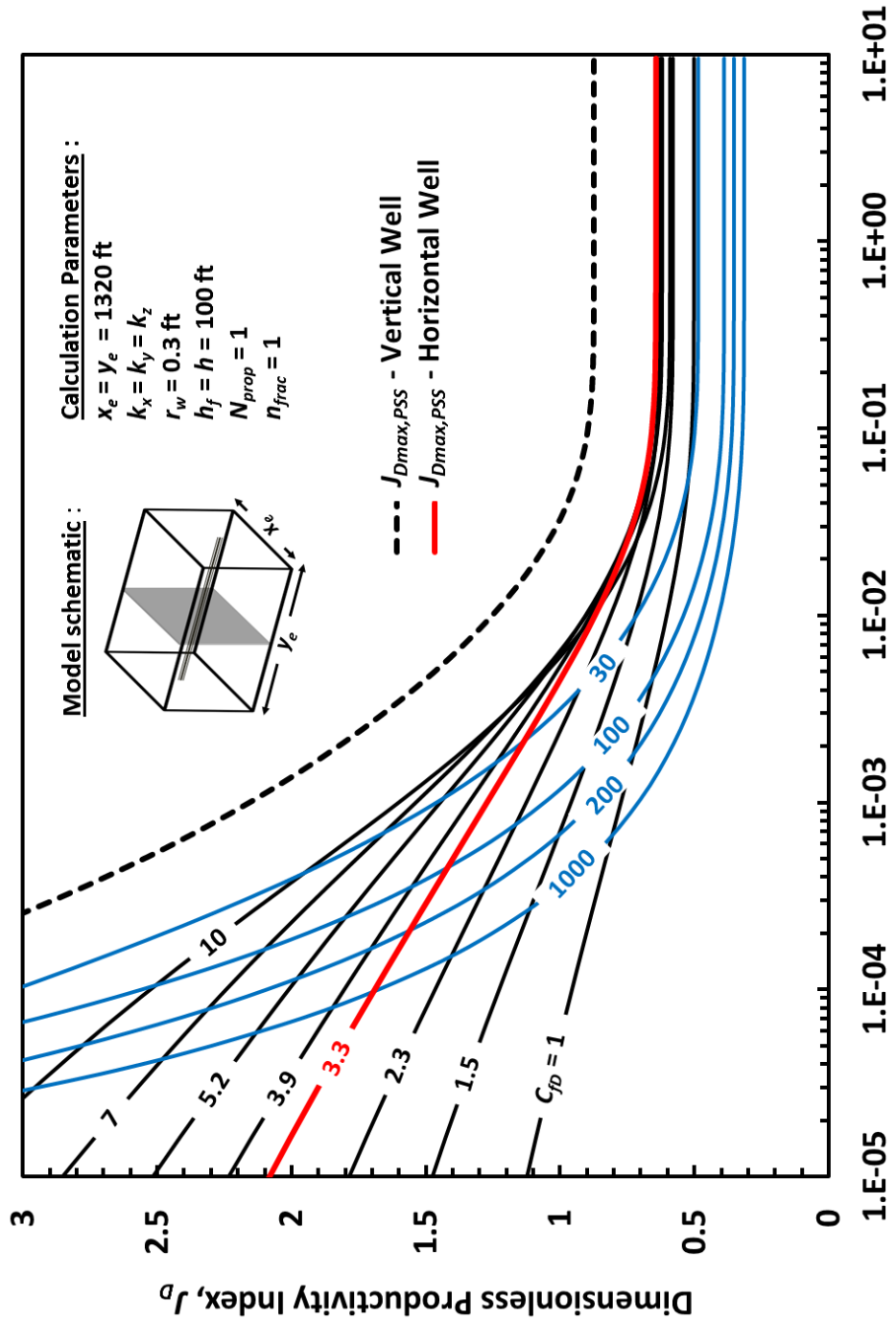

Figure B.3 — Transient and Pseudosteady-state productivity of horizontal well with transverse fracture, N_{prop} = 1

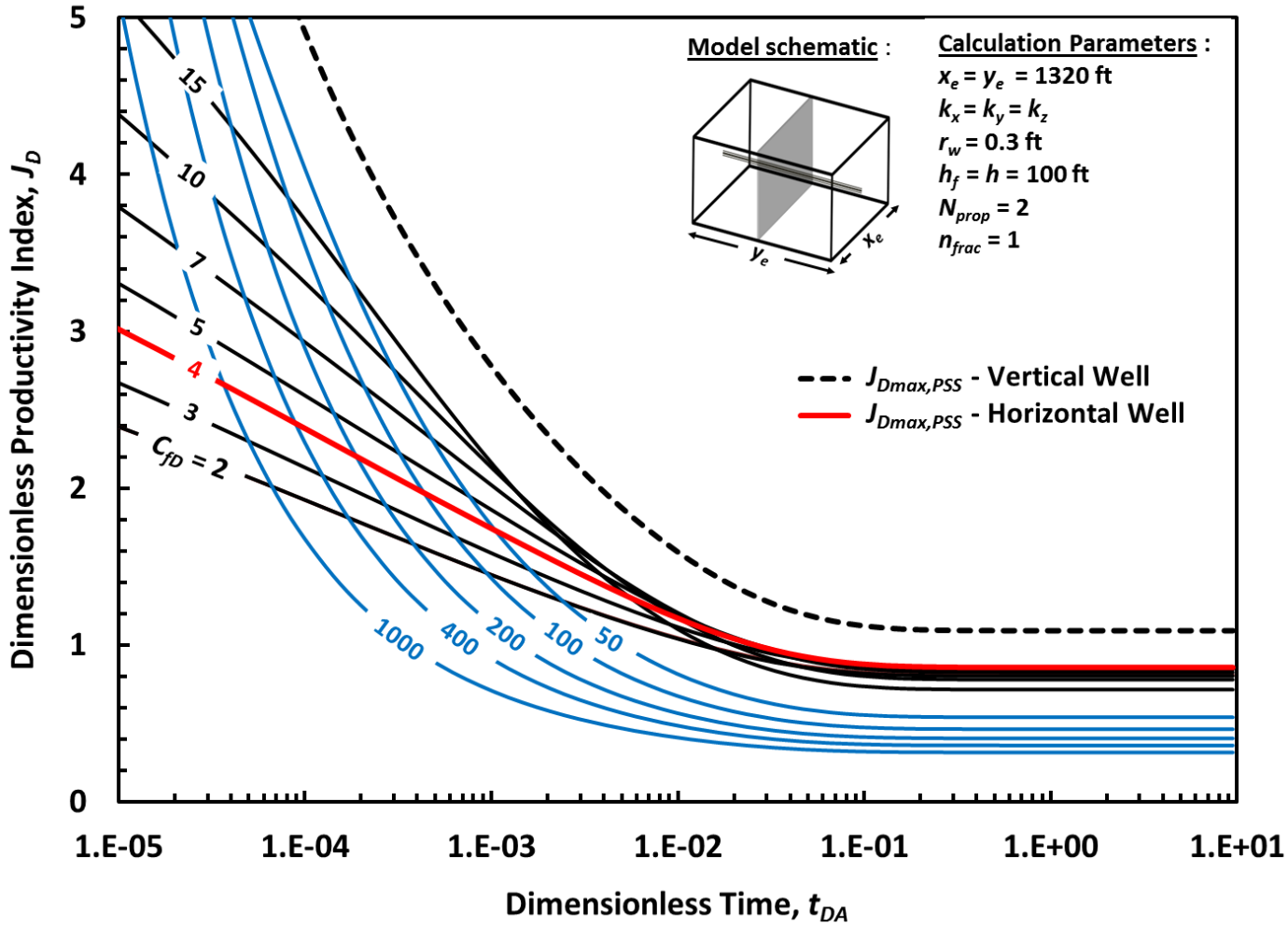

Figure B.4 — Transient and Pseudosteady-state productivity of horizontal well with transverse fracture, N_{prop} = 2

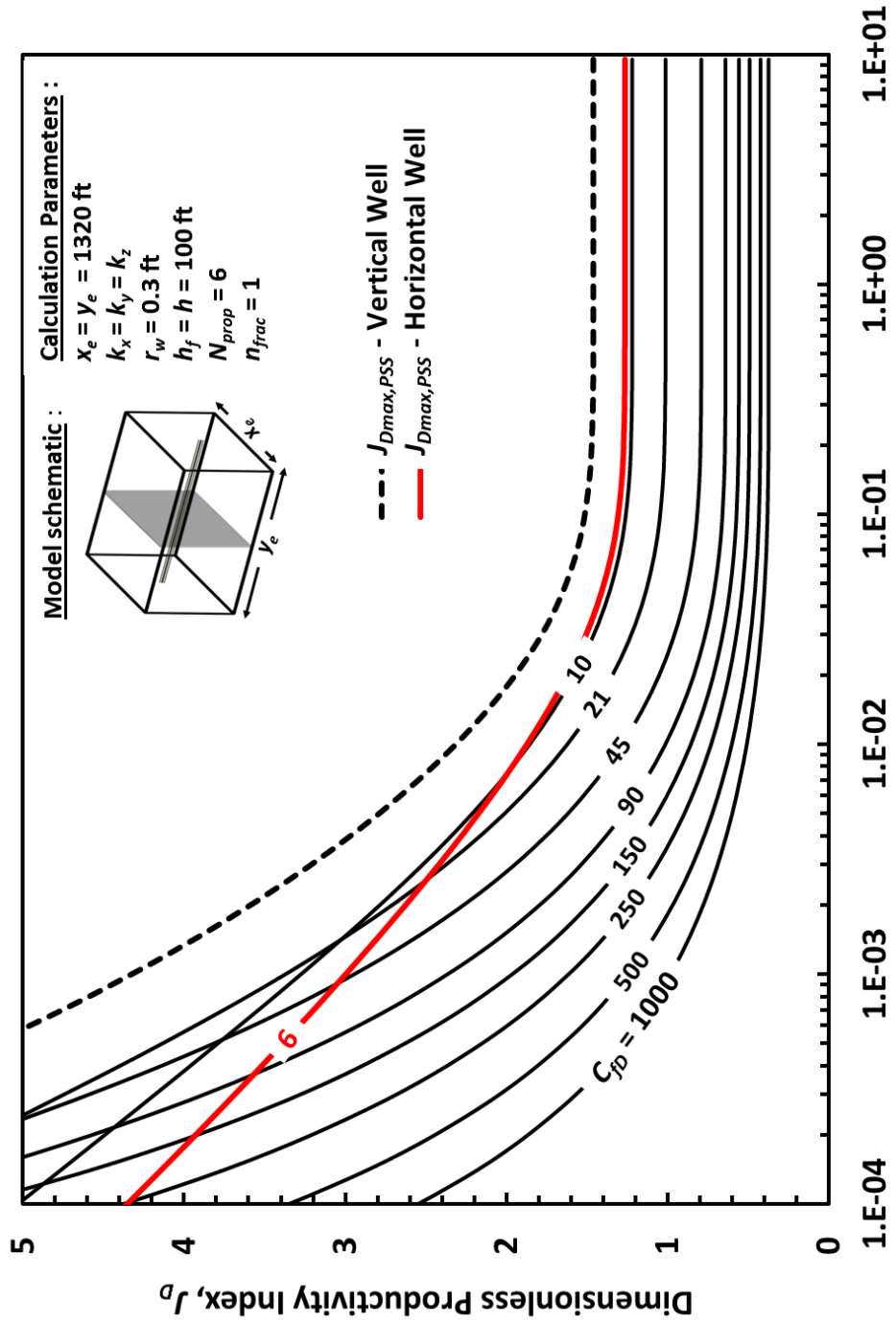

Figure B.5 — Transient and Pseudosteady-state productivity of horizontal well with transverse fracture, N_{prop} = 6

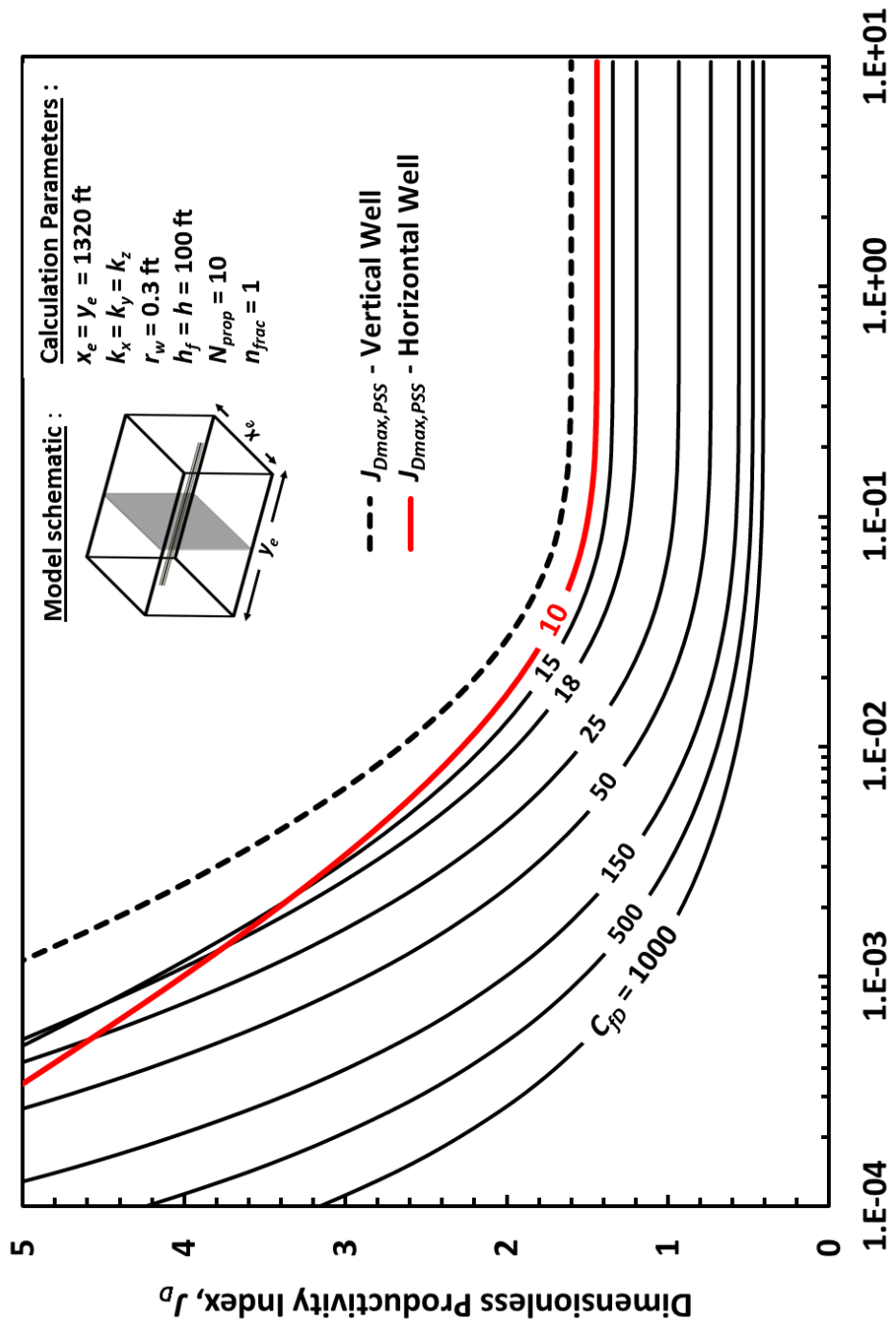

Figure B.6 — Transient and Pseudosteady-state productivity of horizontal well with transverse fracture, N_{prop} = 10

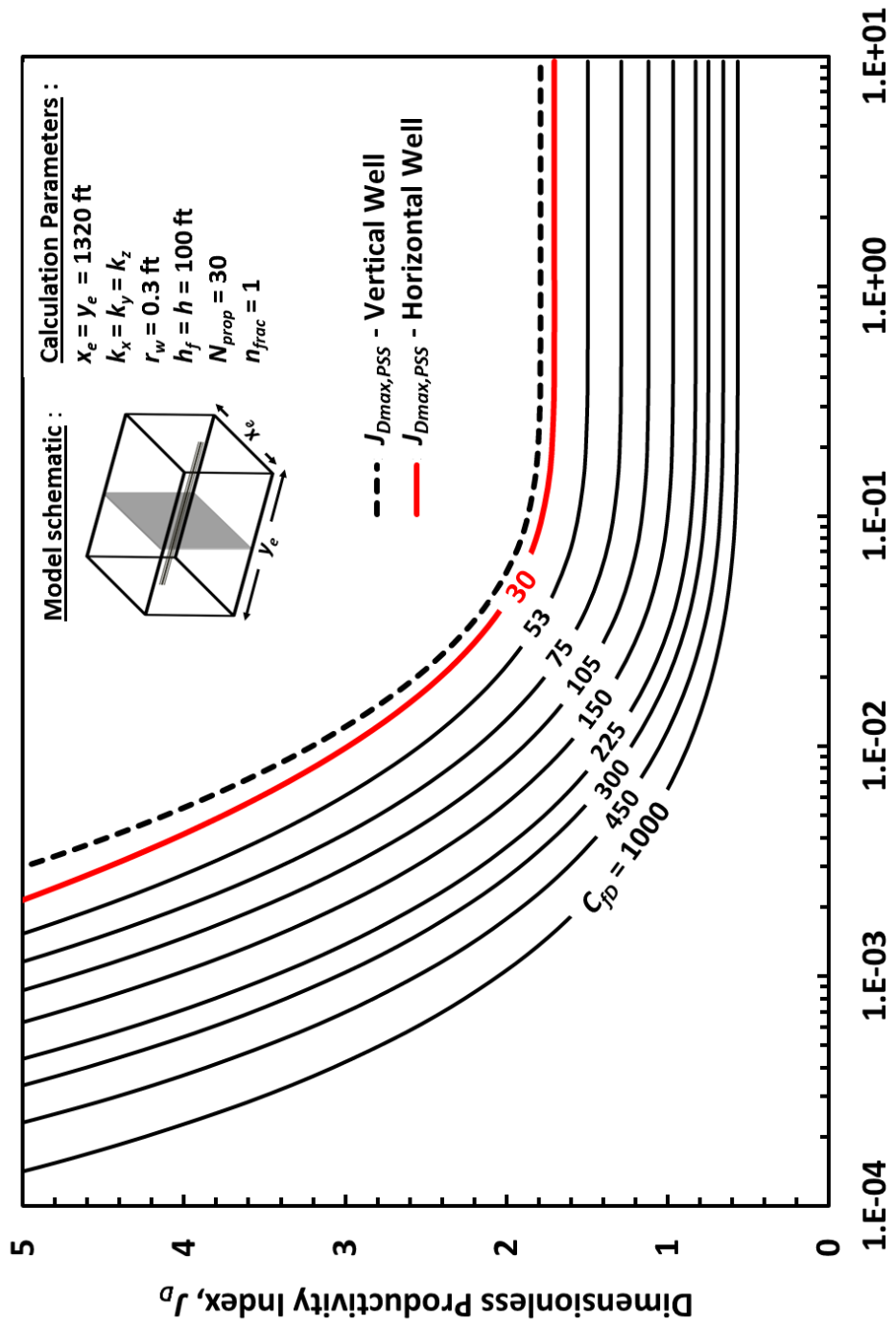

Figure B.7 — Transient and Pseudosteady-state productivity of horizontal well with transverse fracture, N_{prop} = 30

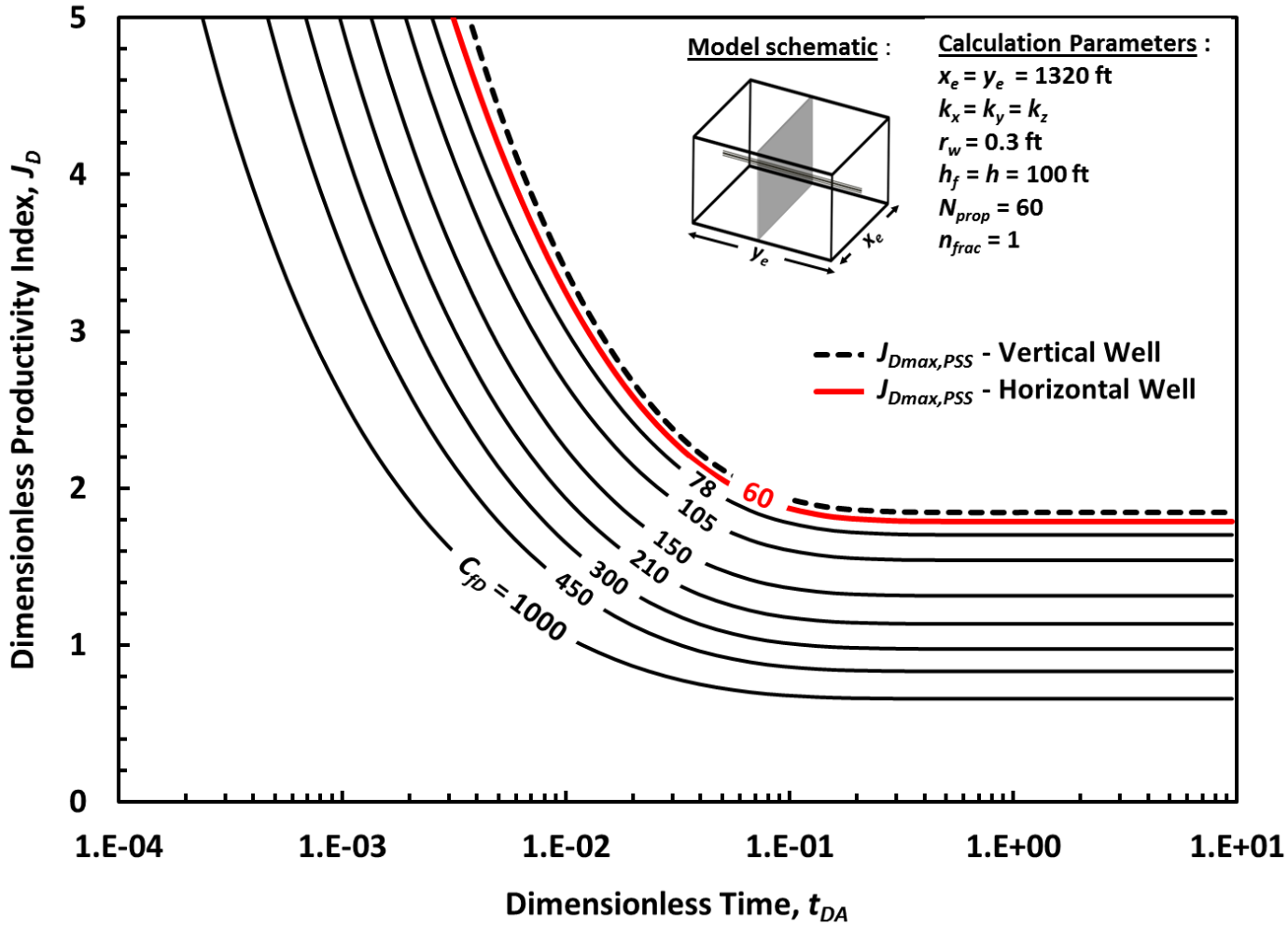

Figure B.8 — Transient and Pseudosteady-state productivity of horizontal well with transverse fracture, N_{prop} = 60

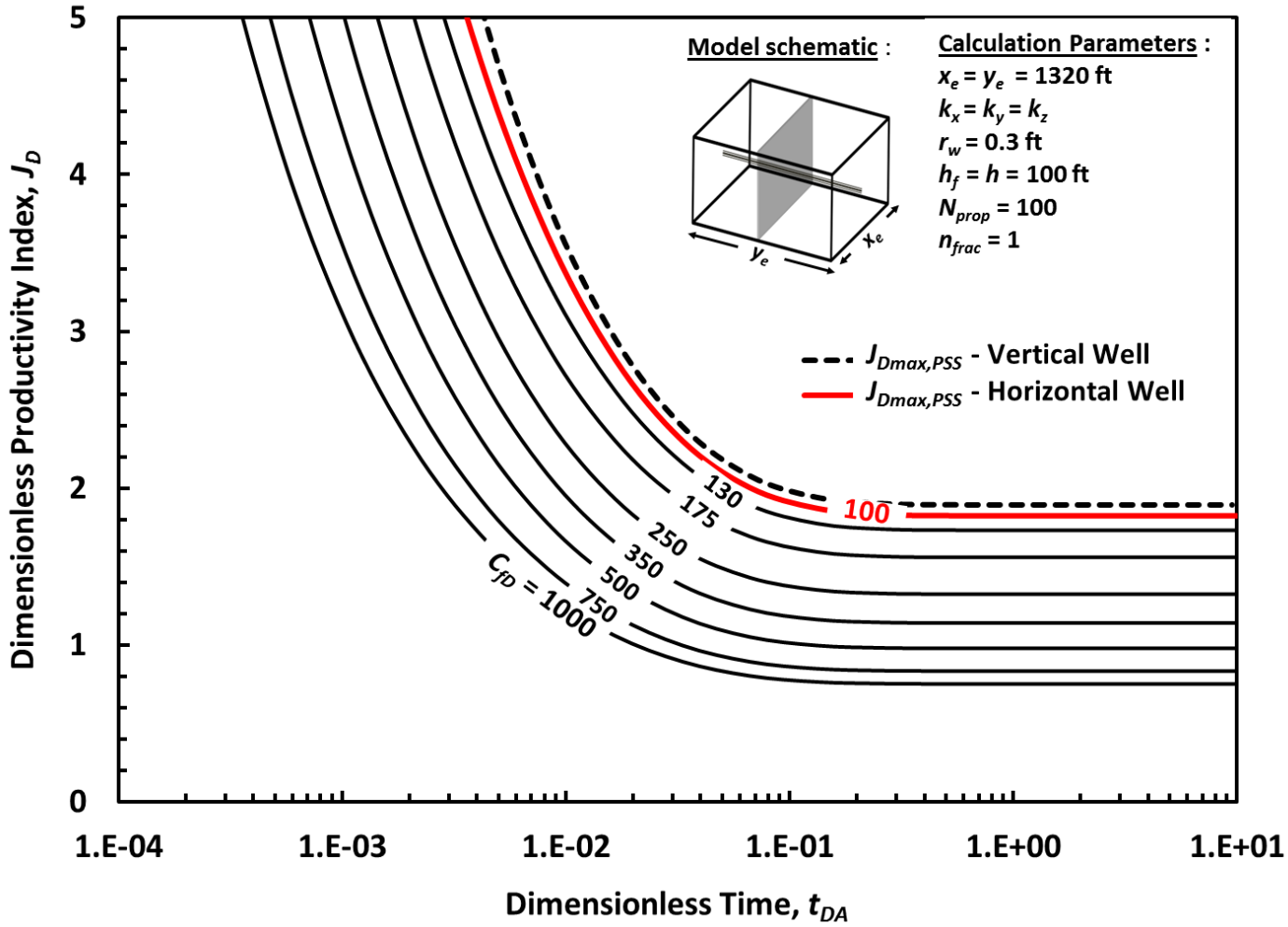

Figure B.9 — Transient and Pseudosteady-state productivity of horizontal well with transverse fracture, N_{prop} = 100

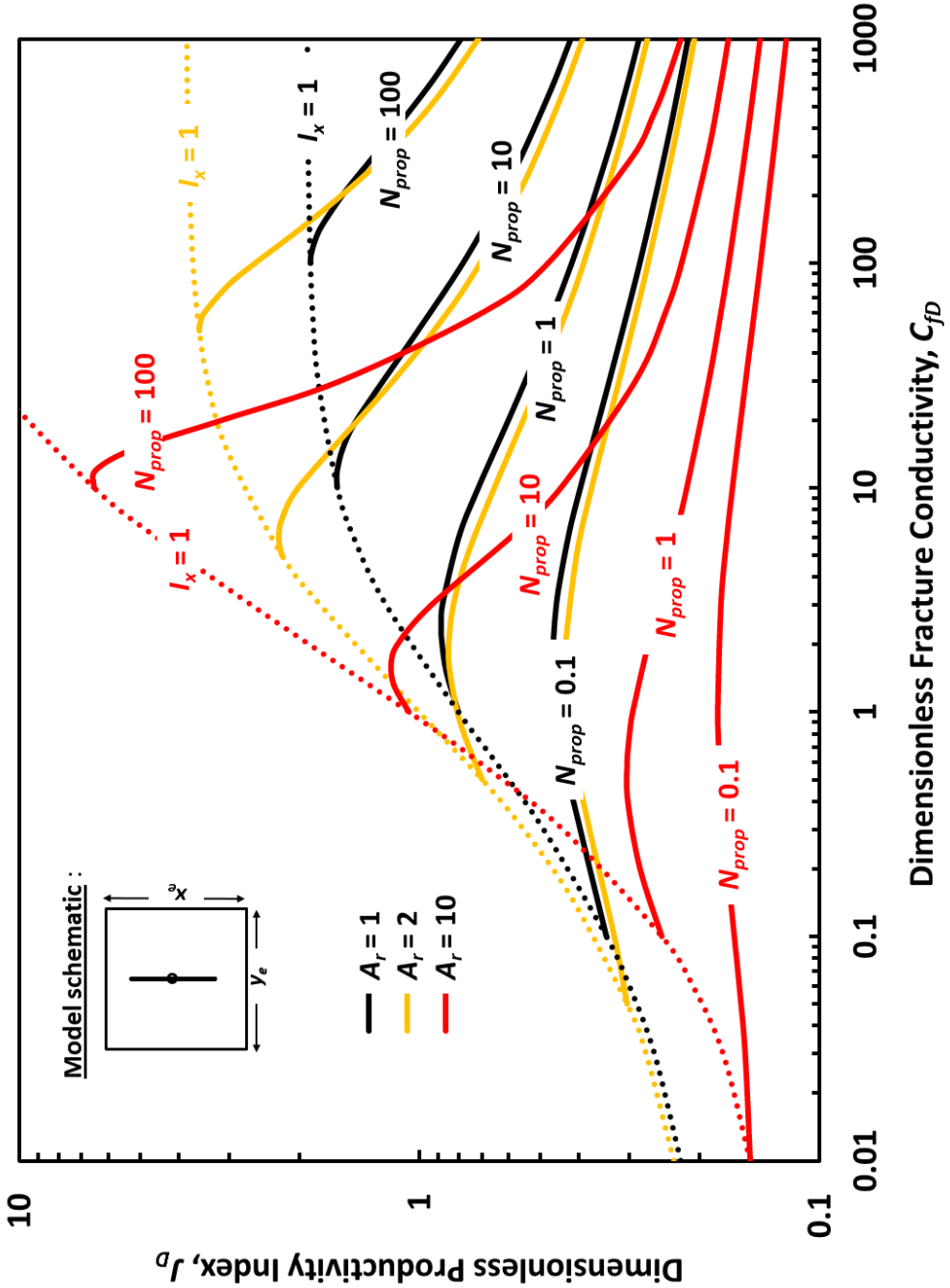

Figure B.10 — Productivity of vertical well intersected by fully penetrating vertical fracture for various aspect ratios and proppant numbers

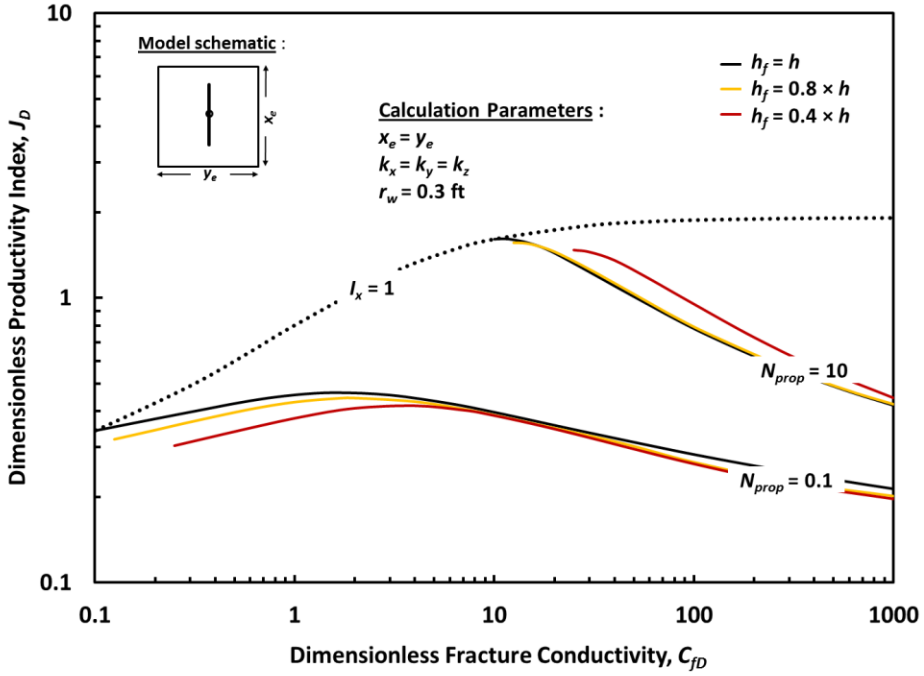

Figure B.11 — Productivity of vertical well intersected vertical fracture for various vertical penetration and proppant numbers

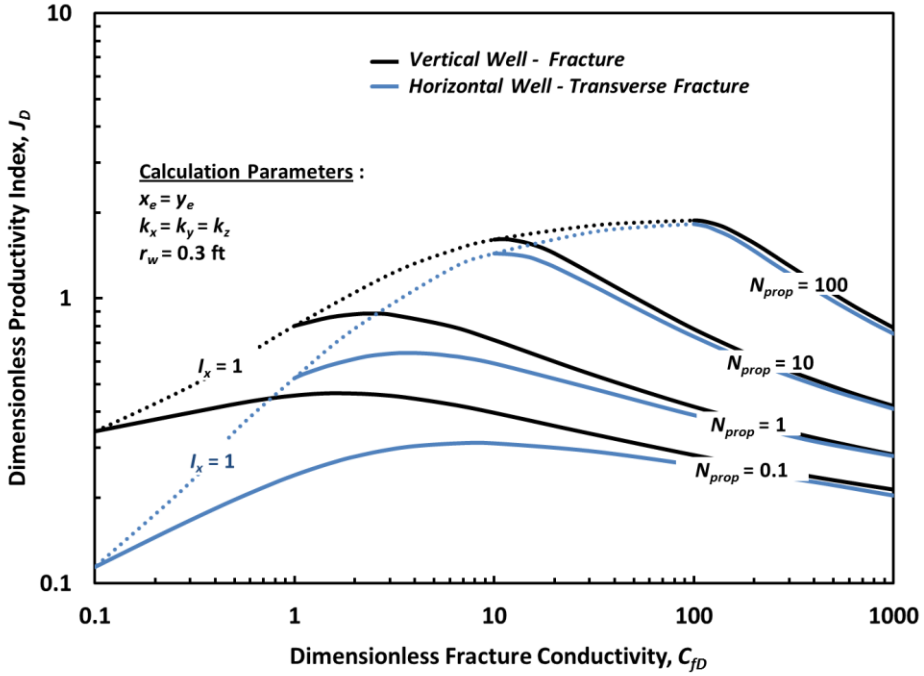

Figure B.12— Productivity comparison of fractured vertical well and horizontal well with transverse fracture with various proppant numbers

APPENDIX C

RESULTS OF CALCULATION FOR DIMENSIONLESS PRODUCTIVITY INDEX OF THE EXAMPLE CASE

Table C.1 Productivity for example case with reservoir anisotropy

n_{frac}	x_f, (ft)	w, (ft)	$h_{f,(ft)}$	N_{prop}	$k_v = k_h$		$k_v = 0.1\,k_h$		$k_v = 0.01\,k_h$	
					J_D	$J_{D\,total}$	J_D	$J_{D\,total}$	J_D	$J_{D\,total}$
1	660	0.066	100	1	0.502	0.502	0.501	0.501	0.501	0.501
1	622.3	0.070	100	1	0.543	0.543	0.542	0.542	0.542	0.542
1	641.1	0.070	97	1	0.538	0.538	0.537	0.537	0.536	0.536
1	660	0.070	94.2	1	0.536	0.536	0.534	0.534	0.532	0.532
1	544.5	0.080	100	1	0.580	0.580	0.580	0.580	0.580	0.580
1	602.3	0.080	90.4	1	0.572	0.572	0.569	0.569	0.564	0.564
1	660	0.080	82.6	1	0.561	0.561	0.555	0.555	0.542	0.542
1	484	0.090	100	1	0.606	0.606	0.606	0.606	0.606	0.606
1	572	0.090	84.6	1	0.599	0.599	0.594	0.594	0.581	0.581
1	660	0.090	73.4	1	0.580	0.580	0.569	0.569	0.541	0.541
1	435.6	0.100	100	1	0.622	0.622	0.621	0.621	0.621	0.621
1	547.8	0.100	79.6	1	0.621	0.621	0.613	0.613	0.592	0.592
1	660	0.100	66	1	0.595	0.595	0.577	0.577	0.535	0.535
2	660	0.034	100	1	0.356	0.711	0.354	0.709	0.354	0.708
2	544.5	0.040	100	1	0.423	0.845	0.421	0.842	0.421	0.842
2	602.3	0.040	90.4	1	0.414	0.828	0.412	0.823	0.408	0.815
2	660	0.040	82.6	1	0.383	0.767	0.379	0.758	0.371	0.742
2	435.6	0.050	100	1	0.478	0.956	0.477	0.953	0.476	0.953
2	547.8	0.050	79.6	1	0.466	0.932	0.460	0.919	0.445	0.890
2	660	0.050	66	1	0.444	0.888	0.430	0.860	0.400	0.800
2	363	0.060	100	1	0.520	1.040	0.519	1.038	0.519	1.038
2	511.5	0.060	71	1	0.506	1.012	0.493	0.987	0.464	0.928
2	660	0.060	55	1	0.461	0.923	0.438	0.876	0.388	0.777
2	311.1	0.070	100	1	0.541	1.083	0.541	1.081	0.541	1.081
2	485.6	0.070	64	1	0.537	1.074	0.517	1.034	0.471	0.942
2	660	0.070	47.2	1	0.490	0.980	0.457	0.914	0.392	0.783
2	272.3	0.080	100	1	0.556	1.113	0.556	1.112	0.556	1.111
2	466.1	0.080	58.4	1	0.562	1.123	0.535	1.071	0.476	0.953
2	660	0.080	41.2	1	0.504	1.007	0.461	0.922	0.382	0.763
2	242	0.090	100	1	0.559	1.118	0.559	1.117	0.558	1.117
2	451	0.090	53.6	1	0.581	1.162	0.547	1.094	0.473	0.946
2	660	0.090	36.6	1	0.514	1.028	0.465	0.929	0.375	0.750
2	217.8	0.100	100	1	0.556	1.112	0.556	1.111	0.555	1.111
2	438.9	0.100	49.6	1	0.597	1.194	0.555	1.111	0.467	0.935
2	660	0.100	33	1	0.523	1.045	0.466	0.933	0.368	0.735

Table C.1 Continued

n_{frac}	x_f, (ft)	w, (ft)	$h_{f,(ft)}$	N_{prop}	$k_v = k_h$		$k_v = 0.1\,k_h$		$k_v = 0.01\,k_h$	
					J_D	$J_{D\,total}$	J_D	$J_{D\,total}$	J_D	$J_{D\,total}$
4	660	0.016	100	1	0.201	0.804	0.199	0.798	0.199	0.796
4	544.5	0.020	100	1	0.255	1.021	0.253	1.014	0.253	1.012
4	602.3	0.020	90.4	1	0.251	1.003	0.249	0.994	0.246	0.985
4	660	0.020	82.6	1	0.230	0.922	0.227	0.910	0.223	0.893
4	363	0.030	100	1	0.327	1.307	0.325	1.302	0.325	1.300
4	511.5	0.030	71	1	0.316	1.263	0.308	1.234	0.292	1.170
4	660	0.030	55	1	0.271	1.085	0.257	1.027	0.227	0.908
4	272.3	0.040	100	1	0.368	1.471	0.367	1.466	0.366	1.466
4	466.1	0.040	58.4	1	0.359	1.437	0.345	1.379	0.311	1.242
4	660	0.040	41.2	1	0.304	1.216	0.270	1.079	0.230	0.919
4	217.8	0.050	100	1	0.387	1.546	0.386	1.543	0.386	1.543
4	438.9	0.050	49.6	1	0.390	1.559	0.367	1.467	0.313	1.253
4	660	0.050	33	1	0.326	1.303	0.295	1.179	0.236	0.943
4	181.5	0.060	100	1	0.393	1.573	0.393	1.571	0.393	1.570
4	420.8	0.060	43.2	1	0.411	1.643	0.380	1.521	0.310	1.242
4	660	0.060	27.6	1	0.340	1.360	0.301	1.205	0.231	0.924
4	155.6	0.070	100	1	0.393	1.571	0.392	1.570	0.392	1.570
4	407.8	0.070	38.2	1	0.426	1.706	0.388	1.554	0.304	1.218
4	660	0.070	23.6	1	0.347	1.389	0.303	1.211	0.226	0.903
4	136.1	0.080	100	1	0.389	1.555	0.388	1.554	0.388	1.554
4	398.1	0.080	34.2	1	0.439	1.754	0.393	1.574	0.297	1.189
4	660	0.080	20.6	1	0.353	1.411	0.303	1.212	0.220	0.882
4	121	0.090	100	1	0.383	1.532	0.383	1.531	0.383	1.531
4	390.5	0.090	31	1	0.447	1.790	0.396	1.583	0.290	1.159
4	660	0.090	18.4	1	0.358	1.431	0.304	1.215	0.217	0.867
4	108.9	0.100	100	1	0.377	1.506	0.376	1.505	0.376	1.505
4	384.5	0.100	28.4	1	0.455	1.818	0.397	1.588	0.283	1.132
4	660	0.100	16.6	1	0.360	1.441	0.303	1.212	0.213	0.853

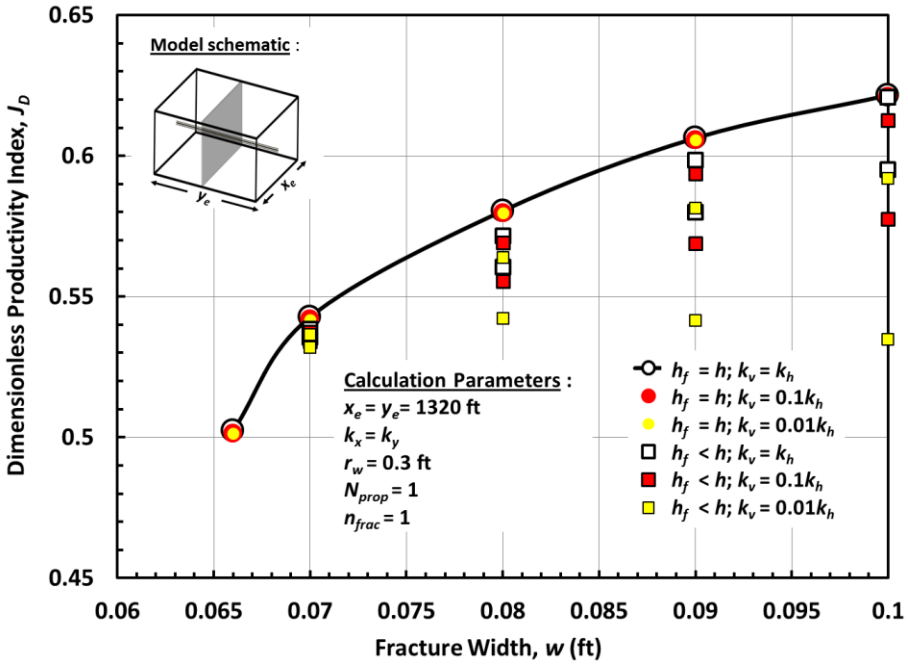

Figure C.1 — Productivity of example case as a function of fracture width with various reservoir anisotropy, $n_{frac} = 1$

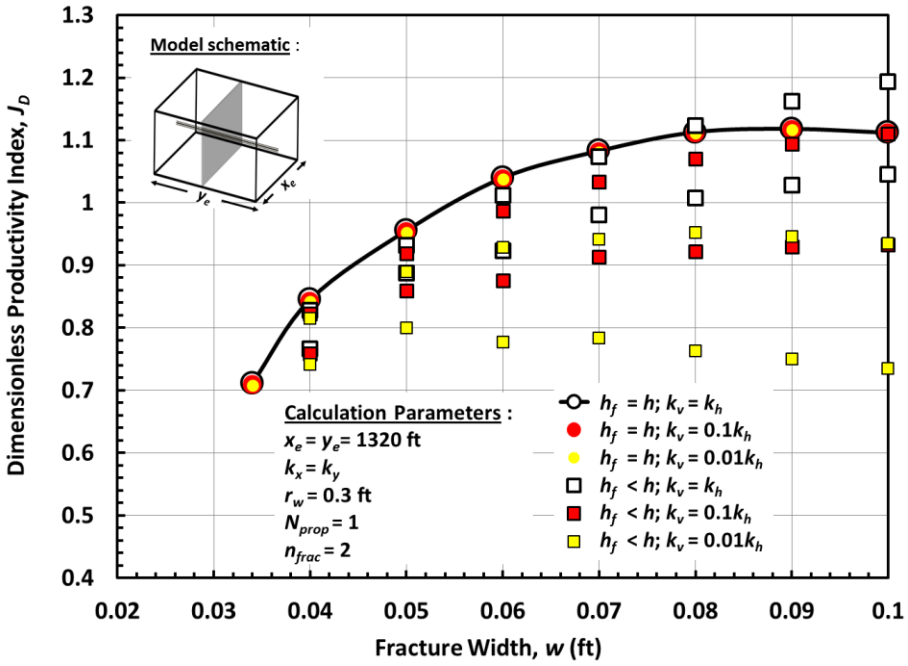

Figure C.2 — Productivity of example case as a function of fracture width with various reservoir anisotropy, $n_{frac} = 2$

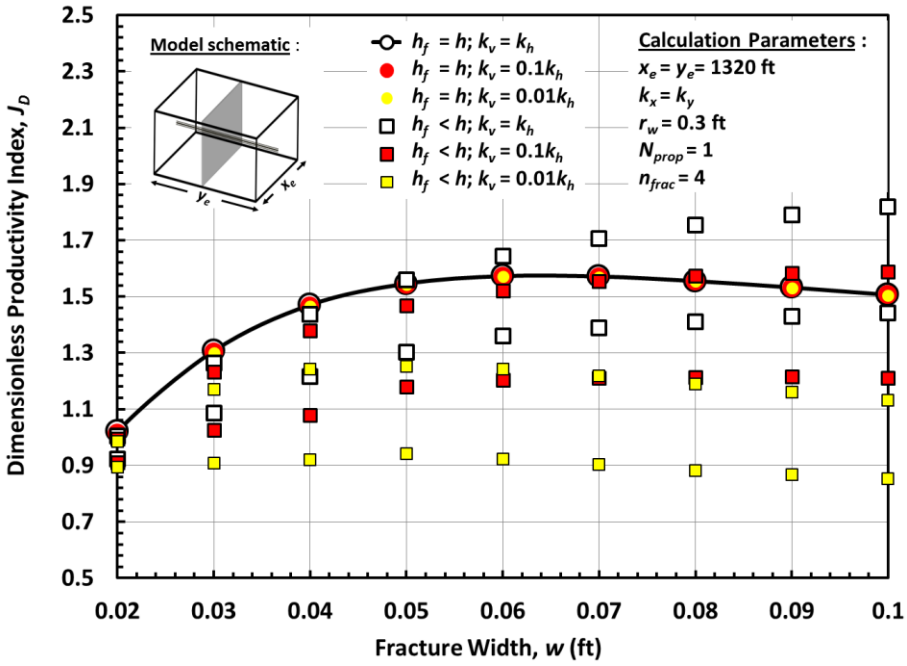

Figure C.3 — Productivity of example case as a function of fracture width with various reservoir anisotropy, $n_{frac} = 4$

VITA

Name:	Ardhi Hakim Lumban Gaol
Address:	Harold Vance Dept. of Petroleum Engineering, Texas A&M University, College Station, TX 77843-3116.
Email Address:	ardhi.lumbangaol@gmail.com
Education:	B.S., Petroleum Engineering, Bandung Institute of Tech, 2009 MS., Petroleum Engineering, Texas A&M University, 2012 College Station, Texas, USA